Applied Thermal Engineering 265 (2025) 125210



Contents lists available at ScienceDirect

Applied Thermal Engineering

journal homepage: www.elsevier.com/locate/apthermeng



Research Paper

Bayesian uncertainty quantification in temperature simulation of borehole heat exchanger fields for geothermal energy supply

Hesam Soltan Mohammadi [a,*], Lisa Maria Ringel [a,b], Christoph Bott [a], Selçuk Erol [c], Peter Bayer [a]

[a] Department of Applied Geology, Institute of Geosciences and Geography, Martin Luther University Halle-Wittenberg, Von-Seckendorff-Platz 3, 06120, Halle (Saale), Germany
[b] Univ. Rennes, CNRS, Géosciences Rennes, UMR 6118, 35000 Rennes, France
[c] Department of Energy Systems Engineering, Engineering Faculty, Izmir Institute of Technology (IZTECH), 35430 Urla-Izmir, Turkey

ARTICLE INFO

Keywords:
Stochastic modeling
Closed-loop geothermal systems
Data assimilation
Bayesian inference
Heat transfer

ABSTRACT

Accurate temperature prediction is crucial for optimizing the performance of borehole heat exchanger (BHE) fields. This study introduces an efficient Bayesian approach for improving the forecast of temperature changes in the ground caused by the operation of BHEs. The framework addresses the complexities of multi-layer subsurface structures and groundwater flow. By utilizing an affine invariant ensemble sampler, the framework estimates the distribution of key parameters, including heat extraction rate, thermal conductivity, and Darcy velocity. Validation of the proposed methodology is conducted through a synthetic case involving four active and one inactive BHE over five years, using monthly temperature changes around BHEs from a detailed numerical model as a reference. The moving finite line source model with anisotropy is employed as the forward model for efficient temperature approximations. Applying the proposed methodology at a monthly resolution for less than three years reduces uncertainty in long-term predictions by over 90%. Additionally, it enhances the applicability of the employed analytical forward model in real field conditions. Thus, this advancement offers a robust tool for stochastic prediction of thermal behavior and decision-making in BHE systems, particularly in scenarios with complex subsurface conditions and limited prior knowledge.

1. Introduction

As part of the ongoing transition to more sustainable and renewable energy sources, shallow geothermal systems present an attractive solution for heating and cooling buildings [1]. These systems use the relatively stable temperatures found at depths ranging from a few tens to hundreds of meters in the subsurface. At the core of these systems are borehole heat exchangers (BHEs), which typically consist of high-density polyethylene (HDPE) pipes arranged in U-pipe, coaxial, or double U-pipe configurations [2]. A heat transfer fluid circulates through these pipes, absorbing heat from the ground in the cold season to supply buildings with heat, and returning excess heat from buildings to the subsurface in the warm season [3]. Although BHEs are established technologies, their efficiency and ability to meet energy demands heavily rely on precise planning. This is because BHE systems are influenced by variable factors such as seasonal variations and time-dependent, coupled physical processes in the subsurface. Therefore, simulating these systems for a reliable prediction of underground thermal behavior is crucial. Accurate predictions can help avoid issues like thermal imbalance, where excessive heat extraction or injection deteriorates the system's efficiency over time. Additionally, models can assist in assessing the environmental impact and ensure that a BHE system operates sustainably throughout its intended lifespan. For example, Chen et al. [4] examined the underperformance of a 56-BHE field implemented in Leicester, UK. They concluded that thermal anomalies in the center of the field prevent the system from operating efficiently for more than two decades.

Aside from technical issues, the thermally imbalanced operation of a BHE field can violate regulations. Haehnlein et al. [5] and Tsagarakis et al. [6] surveyed the legal frameworks for shallow geothermal applications in different countries. Existing frameworks and guidelines are diverse, and they delineate acceptable application windows constrained by factors such as temperature thresholds [7,8]. Blum et al. [9] warned that unplanned, continuous thermal exploitation of the shallow subsurface can lead to heat or cold being deemed as a pollutant. Reliable

* Corresponding author.
E-mail address: hesam.soltan-mohammadi@geo.uni-halle.de (H. Soltan Mohammadi).

https://doi.org/10.1016/j.applthermaleng.2024.125210
Received 9 September 2024; Received in revised form 6 December 2024; Accepted 9 December 2024
Available online 12 December 2024
1359-4311/© 2024 The Author(s). Published by Elsevier Ltd. This is an open access article under the CC BY-NC-ND license (http://creativecommons.org/licenses/by-nc-nd/4.0/).

Nomenclature

a	Thermal diffusivity (m^2s^{-1})
a	Affine invariant step size
A	Acceptance probability
c	Specific heat capacity ($J\,kg^{-1}K^{-1}$)
d	Data
erfc	Complementary error function
$\mathcal{F}$	Forward model
H	Borehole length (m)
ℓ	Log-likelihood
L	Characteristic length (m)
N	Number of measurements
p	Probability
Pé	Péclet number
q	Heat exchange rate (Wm^{-1})
r	Radial distance of observation point (m)
s	Uniform random sample
t	Time (s)
u	Darcy velocity (ms^{-1})
U	Uniform probability distribution
v	Heat transfer velocity (ms^{-1})
x, y, z	Coordinates
z	Affine invariant stretch move

Greek symbols

α_l	Longitudinal dispersivity (m)
α_t	Transversal dispersivity (m)
ΔT	Temperature change (K)
θ	Parameters of interest
λ	Thermal conductivity ($W\,m^{-1}K^{-1}$)
ρ	Density ($kg\,m^3$)
σ	Standard deviation
ϕ	Porosity

Subscripts

1, 2, 3	Layer number
c	Composite
I	Imaginary segment
m	Medium
meas	Measured
R	Real segment
s	Solid
w	Water

long-term predictions are therefore needed to assess compliance with precautionary regulations while ensuring safe and cost-efficient operation.

A wide variety of modeling tools has been developed to predict the thermal state, both inside and outside of BHEs. These tools range from analytical and semi-analytical to fully numerical methods. (Semi-) analytical solutions, such as those based on the so-called g-functions, offer simplified, closed-form formulations that allow for a quick approximation of the subsurface thermal response [10]. While these models efficiently reflect overall system thermal performance, they have limitations when applied to complex subsurface structures with heterogeneous material properties or coupled heat transport processes. Although efforts have been made to extend the applicability of (semi-) analytical models to account for multi-layer subsurface [11], advective heat transport e.g., due to groundwater flow [12], land use effects and surface ground conditions [13,14], and heterogeneous-discontinuous thermal loads [15], the majority of existing analytical models still have conceptual simplifications. Alternatively, numerical models enable detailed simulations by solving complex heat transfer equations under more realistic boundary conditions [16–23]. Numerical methods are beneficial for the design phase and initial planning, but it remains a challenge to choose a flexible and computationally efficient predictive model for real-time optimization and control of BHE fields [24,25].

To simulate BHEs' performance analytically or numerically, ground properties must be characterized as a prerequisite. For this purpose, thermal response tests (TRTs) are usually performed at the beginning of the operation to determine the thermal properties of the subsurface, such as thermal conductivity, heat capacity, and thermal resistivity [26,27]. However, these early-phase experiments often provide only a snapshot of subsurface conditions and cannot fully capture the complex, dynamic nature of subsurface heat transfer over time. Factors such as seasonal temperature fluctuations, transient groundwater movement, and long-term thermal interactions between BHEs within a field can significantly alter the thermal conditions in the subsurface, which initial TRT results are not able to resolve. Ideally, regular monitoring and continuous updating of subsurface models of BHE fields would be needed to account for uncertainties in model parameters or model simplifications [28].

When inferring subsurface thermal parameters or g-functions from TRTs, parameter identification typically involves defining a mathematical minimization problem or realizing the statistical distributions of parameters to assess the associated uncertainty. Among model calibration strategies, for example, Dion et al. [29–31], suggest a deconvolution-based framework. This approach directly infers the transfer function from TRT data, eliminating the need for a predefined thermal model. It uses a multi-objective optimization to reconstruct the derivatives of the temperature, allowing for a data-driven construction of g-functions. Aside from this, different types of optimization techniques, such as particle swarm optimization with pattern search [32], or trust region [33] have been explored to calibrate model parameters and improve model predictability. However, these procedures are commonly not applied in the long term, or they do not fully account for the complex conditions of the underground.

While classic model calibration techniques are computationally efficient, capturing the full complexity of subsurface conditions is challenging. This is particularly true when dealing with advective heat transport in heterogeneous ground or when numerous model parameters need to be characterized. Then, ill-posedness of the formulated calibration problem is likely to yield non-unique solutions, as well as insensitive and correlated parameters. Alternatively, probabilistic methods such as Kalman filters can be employed to enhance the accuracy of simulations by dynamically adjusting model parameters based on monitoring data [34,35]. While Kalman filter methods are efficient and capable of real-time updates, they rely on Gaussian assumptions. These can lead to inaccuracies when exploring correlated and non-Gaussian parameter spaces. Moreover, Kalman filters can encounter difficulties in dealing with highly nonlinear systems or when there is significant model misspecification, resulting in suboptimal performance in complex subsurface environments.

Bayesian inference, as another probabilistic approach, represents a promising alternative, especially through methods like Markov Chain Monte Carlo (MCMC). Unlike classic calibration methods, Bayesian inference does not merely seek to identify optimal parameter values or assume a specific distribution for the model parameters. Instead, it samples from the posterior distribution to explore a wide range of probable parameter sets.

In several studies, Bayesian frameworks have been employed to estimate subsurface thermal conductivity and borehole thermal resistance, along with the associated uncertainties [36,37]. Their findings highlighted the importance of test duration in enhancing the accuracy of the estimates. In other attempts, Bayesian methods have also been used to distinguish between errors arising from the TRT experiments and those

stemming from the model structure itself to explicitly quantify the model bias [38,39]. To further improve computational efficiency in Bayesian inference, Pasquier and Marcotte [40] developed a new closed-form likelihood formulation combined with neural networks which also addresses temporal correlations in TRTs for inference of five parameters.

As recently demonstrated by Shin et al. [41] through a global sensitivity analysis, the contribution of parameters in uncertainty assessment changes temporally during BHE operation, underscoring the need for dynamic uncertainty assessments in BHE systems. However, the majority of previous studies on the long-term thermal evolution of BHE fields have concentrated on developing sophisticated modeling tools rather than utilizing data assimilation techniques. With advancements in measurement technologies, such as distributed temperature sensing (DTS), there is an opportunity to better harness high-resolution subsurface data. This can be used to enhance model predictability and reduce input parameter uncertainty over the long term, particularly in cases involving complex subsurface structures and coupled processes [42,43].

To address this scientific gap, this work introduces a new Bayesian inference-based framework that learns during operation and models the thermal evolution of BHE fields in a stochastic manner. In particular, this work focuses on conditions with stratified subsurface heterogeneity in the presence of groundwater over five years of operation. This framework integrates temperature measurements taken from the synthetic BHE field at defined time intervals to infer the statistical distributions of key model parameters, such as heat extraction rates, Darcy velocity, and thermal conductivity for each layer.

By characterizing these statistical distributions, a robust measure is achieved for assessing uncertainties in the model's predictions based on the most likely input parameter sets. The incorporation of temperature measurements reflects the true thermal state, which refines the predictive model, reduces uncertainties, and improves predictive accuracy. The continuous updating process is a core strength of the Bayesian approach, allowing dynamic adaptation of model parameters in response to new information.

The presented framework employs the moving finite line source model with anisotropy (MFLSA) as the forward model [44]. This model is particularly well-suited for BHE systems due to its computational efficiency, enabling the rapid evaluation of different parameter proposals during the Bayesian inference process. The MFLSA simulates the thermal state at the monitoring location in an operating field, considering the layered structure of the subsurface and the influence of groundwater flow. This accounts for variability and uncertainty in boundary conditions, changes in operational settings, and other unforeseen fluctuations in the system. A conceptual illustration of the proposed framework is presented in Fig. 1.

The proposed methodology introduces several important advancements in modeling and analysis of the thermal behavior in closed-loop geothermal systems. Its primary contribution is an extension of probabilistic modeling to simulate temperature changes in the subsurface surrounding a BHE field over multiple years of operation. Additionally, the Bayesian framework is designed to effectively manage the highly correlated, high-dimensional parameter space associated with conductive-advective heat transport in a multi-layered subsurface, focusing on operational thermal simulation rather than using the inversion procedures for site characterization. Furthermore, this work broadens the applicability of analytical finite line source models by relaxing the assumption of a constant heat extraction rate across the layers, thus enhancing the realism of thermal predictions in heterogeneous geological settings.

Building on these advancements, the primary objective of this study is to employ statistical inference to enhance the understanding of thermal state evolution within BHE fields, utilizing high-resolution operational data over time. A secondary objective is to explore the capability of Bayesian inversion to dynamically update model parameters, enabling the model to adaptively reflect observed thermal states rather than developing a new modeling tool with additional constraints.

The structure of this paper is as follows: Section 2 provides an overview of the methodology, including the derivation of the forward model, the details of the Bayesian inference approach, the development of a synthetic case study, and the inversion implementation. The results of this study are presented and discussed in Section 3, followed by conclusions in Section 4.

2. Methodology

2.1. Forward modeling

To assess and reduce uncertainties in predicting temperature changes in a BHE field through a Bayesian framework, a forward model needs to be set up. This model should reproduce the true temperature distribution, enabling the comparison with observed data and iterative refinement of predictions. In this study, a line-source model for BHEs is employed that considers advection and dispersion mechanisms in a

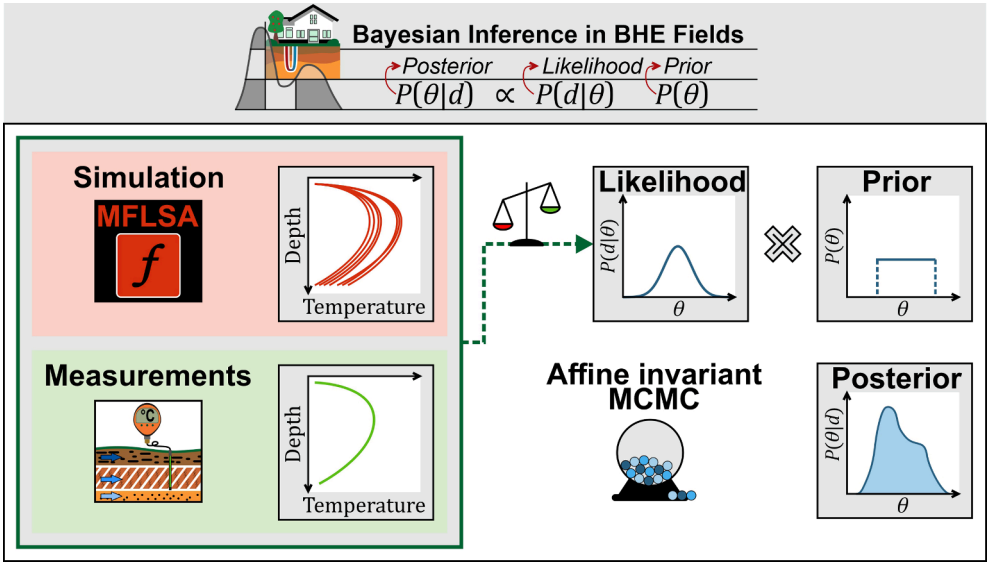


Fig. 1. Conceptual framework of the proposed Bayesian method for stochastic predictions of temperature changes in the BHE field based on temperature measurements and using the MFLSA as the forward model.

multilayer porous medium. In particular, anisotropy is added to the moving finite line source model. Furthermore, a composite computational approach is applied, and layers are subdivided into segments to calculate the temperature difference at a point of interest located in one of the layers. Groundwater flow is separately considered in the layers. The composite method segregates the layers and their thermal properties and adds the calculated temperature differences from each layer. For instance, if the observation point is situated in the first layer, this layer is designated as the first segment, while the other layers are assigned to the second segment (Fig. 2). The temperature difference is computed as follows:

$$\Delta T_1(x,y,z,t) = \frac{q_L}{2\pi\lambda_{y1}} \exp\left[\frac{x v_{T1}}{2a_{x1}}\right]\left[\int_0^{z_1} f(x,y,z,t)dz' - \int_{-z_1}^{0} f(x,y,z,t)dz'\right] \tag{1}$$

q_L is the heat exchange rate. The subscript 1 denotes the first layer and the $f(x,y,z,t)$ is:

$$f(x,y,z,t) = \frac{1}{4r_A}\left[\exp\left(-\frac{v_{T1}r_A}{2a_{x1}}\right)\mathrm{erfc}\left(\frac{r_A - v_{T1}t}{2\sqrt{a_{x1}t}}\right) + \exp\left(\frac{v_{T1}r_A}{2a_{x1}}\right)\mathrm{erfc}\left(\frac{r_A + v_{T1}t}{2\sqrt{a_{x1}t}}\right)\right] \tag{2}$$

in which v_T is the thermal transport velocity that is calculated as:

$$v_{T1} = \frac{\mathrm{Pé} a_{x1}}{L} = u_x \frac{\rho_w c_w}{\rho_m c_m} \tag{3}$$

where a_{x1} is the thermal diffusivity in the first segment $\lambda_x/\rho_m c_m$, L is the characteristic length, and Pé is the Péclet number:

$$\mathrm{Pé} = \frac{u_x \rho_w c_w L}{\lambda_x} \tag{4}$$

Here, u_x is Darcy's velocity in the x-direction. $\rho_m c_m$ is the volumetric heat capacity of the medium, which can be calculated concerning the porosity ϕ as the weighted arithmetic mean of the solids $\rho_s c_s$ and volumetric heat capacity of water $\rho_w c_w$:

$$\rho_m c_m = (1-\phi)\rho_s c_s + \phi \rho_w c_w \tag{5}$$

The components of effective longitudinal and transverse thermal conductivities are defined in the directions of x, y, and z as follows:

$$\lambda_x = \lambda_m + \alpha_l \rho_w c_w u_x \tag{6}$$

$$\lambda_y = \lambda_z = \lambda_m + \alpha_t \rho_w c_w u_x \tag{7}$$

where λ_m is the bulk thermal conductivity of the porous medium in the

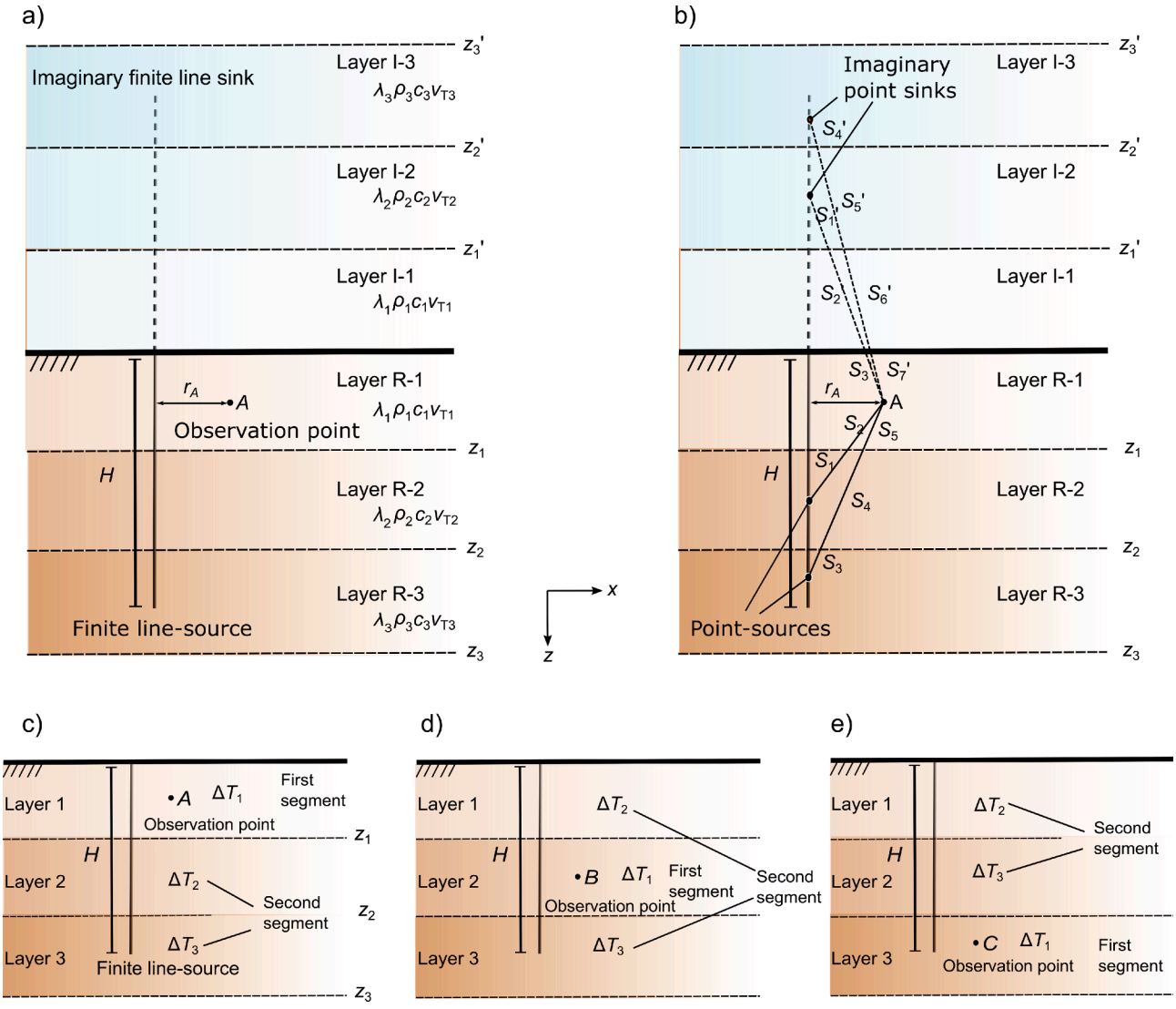


Fig. 2. The illustration of the composite model approach for a single BHE with a finite length of H and its imaginary part passing through multi-layers.

absence of groundwater flow, α_l and α_t are the longitudinal and transverse dispersivities, respectively. The thermal dispersion is a linear function of groundwater flow and relates to the anisotropy of the velocity field.

If groundwater does not exist in a layer, the heat transport velocity v_{T1} becomes zero, and the thermal diffusivity and conductivity values take on isotropic values. The integration limits ([0 z_1] in this case) correspond to the depth coordinates of the BHE in the considered first segment layer with its imaginary part. Two additional layers (i.e., layers 2 and 3) are paired by the second segment. The subsequent layer (layer 2) is calculated as:

$$\Delta T_2(x,y,z,t) = \frac{q_L}{2\pi}\left[\int_{z_1}^{z_2} f_{R2}(x,y,z,t)dz' - \int_{-z_2}^{-z_1} f_{I2}(x,y,z,t)dz'\right] \tag{8}$$

$$f_{R2}(x,y,z,t) = \frac{1}{4\lambda_{cR2}r_A}\exp\left[\frac{xv_{T2}}{2a_{cR2}}\right]\left[\exp\left(-\frac{v_{T2}r_A}{2a_{cR2}}\right)\mathrm{erfc}\left(\frac{r_A - v_{T2}t}{2\sqrt{a_{cR2}t}}\right) + \exp\left(\frac{v_{T2}r_A}{2a_{cR2}}\right)\mathrm{erfc}\left(\frac{r_A + v_{T2}t}{2\sqrt{a_{cR2}t}}\right)\right] \tag{9}$$

The real and the imaginary parts of this mathematical solution are based on the method of images, which is a particular use of Green's functions. When the distribution has a geometric center, such as the point-line source, and the boundary is a flat surface, as shown in Fig. 2, the method of images enables the distribution to be reflected in a straightforward mirror-like manner to fulfill several boundary conditions. For instance, consider the heat distribution as a function of z and a single boundary at z_b. In this case, the real domain is $z \geq z_b$, while the imaginary domain is $z < z_b$.

The subscript c represents the composite and R is the real part of the geometry.

$$f_{I2}(x,y,z,t) = \frac{1}{4\lambda_{cI2}r_A}\exp\left[\frac{xv_{T2}}{2a_{cI2}}\right]\left[\exp\left(-\frac{v_{T2}r_A}{2a_{cI2}}\right)\mathrm{erfc}\left(\frac{r_A - v_{T2}t}{2\sqrt{a_{cI2}t}}\right) + \exp\left(\frac{v_{T2}r_A}{2a_{cI2}}\right)\mathrm{erfc}\left(\frac{r_A + v_{T2}t}{2\sqrt{a_{cI2}t}}\right)\right] \tag{10}$$

where I denotes the imaginary part.

The computation of layer 3 in the second segment is:

$$\Delta T_3(x,y,z,t) = \frac{q_L}{2\pi}\left[\int_{z_2}^{H} f_{R3}(x,y,z,t)dz' - \int_{-H}^{-z_2} f_{I3}(x,y,z,t)dz'\right] \tag{11}$$

where the real part of this function is:

$$f_{R3}(x,y,z,t) = \frac{1}{4\lambda_{cR3}r_A}\exp\left[\frac{xv_{T3}}{2a_{cR3}}\right]\left[\exp\left(-\frac{v_{T3}r_A}{2a_{cR3}}\right)\mathrm{erfc}\left(\frac{r_A - v_{T3}t}{2\sqrt{a_{cR3}t}}\right) + \exp\left(\frac{v_{T3}r_A}{2a_{cR3}}\right)\mathrm{erfc}\left(\frac{r_A + v_{T3}t}{2\sqrt{a_{cR3}t}}\right)\right] \tag{12}$$

and its imaginary part is:

$$f_{I3}(x,y,z,t) = \frac{1}{4\lambda_{cI3}r_A}\exp\left[\frac{xv_{T3}}{2a_{cI3}}\right]\left[\exp\left(-\frac{v_{T3}r_A}{2a_{cI3}}\right)\mathrm{erfc}\left(\frac{r_A - v_{T3}t}{2\sqrt{a_{cI3}t}}\right) + \exp\left(\frac{v_{T3}r_A}{2a_{cI3}}\right)\mathrm{erfc}\left(\frac{r_A + v_{T3}t}{2\sqrt{a_{cI3}t}}\right)\right] \tag{13}$$

The detailed derivation of the model, the composite calculation equations of the thermal properties of layers, and the verification of the analytical solution for different hydraulic and thermal properties by comparison with a numerical solution can be found in [45]. Finally, the temperature difference at the observation point A located in layer 1 is summed up as:

$$\Delta T_A(x,y,z,t) = \Delta T_1 + \Delta T_2 + \Delta T_3 \tag{14}$$

If the observation point is moved to layer 2, then layer 1 and layer 3 can be regarded as being in the second segment computation, by which layer 2 becomes the first segment (Fig. 2d). The same methodology can be used to assess the observation point placed in layer 3 by shifting the segments between layers (Fig. 2e).

The long-term temperature responses of this model over depth and time are validated for the same (hydro)geological scenario investigated in this study using data from [45]. Details are given in the Appendix.

2.2. Inverse modeling

A framework is proposed that leverages Bayes' rule to invert the unknown input model parameters of the MFLSA using monthly temperature changes observed in a BHE field. Specifically, the aim is to quantify the posterior probability distributions of the model parameters $p(\theta|d_{meas})$ by using the measured temperature change data, as expressed by the following relation:

$$p(\theta|d_{meas}) \propto p(d_{meas}|\theta)p(\theta) \tag{15}$$

Here, θ represents the unknown thermal and hydraulic model parameters, which are treated as random variables characterized by a probability density function. The likelihood $p(d_{meas}|\theta)$ quantifies how well the forward model, which simulates temperature changes, agrees with the observed data. The likelihood is assumed to follow a Gaussian distribution, making the log-likelihood function proportional to the sum of squared errors between the simulated and observed temperature changes across all measurement points:

$$\log p\left(d_{meas}|\theta_{1,\cdots,n}\right) \propto -\frac{1}{2\sigma^2 N_{d_{meas}}}\sum_{i=1}^{N_{dmeas}}\left(d_{meas_i} - \mathscr{F}\left(\theta_{1,\cdots,n}\right)_i\right)^2 \tag{16}$$

where $\mathscr{F}\left(\theta_{1,\cdots,n}\right)$ represents the simulated temperature changes computed by the forward model, given a set of n input parameters $\theta_{1,\cdots,n}$. The prior probability distribution function $p(\theta)$ can encapsulate any prior knowledge, assumptions, or conceptual understanding of the model parameters. The prior can be informative, based on previous studies or expert knowledge, or non-informative, such as a uniform distribution, when limited or no prior information is available.

A commonly used method for exploring the target distribution, i.e., the posterior distribution, within the parameter space is MCMC sampling [46]. MCMC generates samples that converge towards the target distribution and thus provide a numerical approximation to the posterior value. Numerous strategies have been developed in the literature to efficiently sample [47]. However, MCMC algorithms can face challenges when the posterior distribution contains sharp correlations in the parameter space and/or when dealing with a highly parameterized space. In these settings, convergence is often intractable, therefore requiring extensive tuning to improve the performance. To tackle this issue, Goodman and Weare [48] introduced the affine invariant ensemble sampler (AIES), an efficient algorithm that performs well under these conditions. The AIES initializes an ensemble of L Markov Chains, known as "walkers", denoted as $\vec{\theta} = \{\theta_1, \cdots, \theta_L\}$, to collectively explore the parameter space. The walkers are set up at distinct starting positions within the parameter space. Subsequently, each walker in the ensemble proposes new candidate parameter values (positions) by perturbing its current value (position) through a "stretch move" mechanism that is invariant to affine transformations of the parameter space. This means that the sampling algorithm's performance is consistent regardless of scaling, rotation, or translation of the target distribution. The proposal for each walker $(\widetilde{\theta}_i)$ is generated based on a random linear combination of the current positions of the walker (θ_i), another randomly chosen complementary walker (θ_j), and an affine invariant stretch move $(\varkappa)$, ensuring that the exploration of the parameter space is robust to different scales and correlations by using:

$$\widetilde{\theta}_i = \theta_j + \varkappa\cdot\left(\theta_i - \theta_j\right) \tag{17}$$

where the "stretch move" is randomly drawn from the following distribution:

$$g(x) \propto \begin{cases} \frac{1}{\sqrt{x}}, & x \in \left[\frac{1}{a}, a\right] \\ 0, & \text{otherwise} \end{cases} \tag{18}$$

The acceptance of the proposed position is determined by comparing the log probabilities of the proposed and current values. The Metropolis-Hastings acceptance criterion is used as:

$$\log\left(\frac{p\left(d_{meas}|\tilde{\theta}_i\right)}{p(d_{meas}|\theta_i)}\right) > \log\ (s) \tag{19}$$

where p denotes the probability density, and $s \sim \mathrm{U}(0,1)$. The schematic workflow of the sampling procedure is shown in Fig. 3.

2.3. Model setup for the demonstration case

This study explores a synthetic BHE field to demonstrate the uncertainty quantification. The setup comprises four active BHEs and one inactive BHE, as illustrated in Fig. 4. The active BHEs operate only in heating mode to meet thermal demands, while the inactive BHE functions as a DTS monitoring site, collecting data on subsurface temperature changes caused by the heating operation of the active BHEs, following a similar configuration as in [43]. Throughout this study, temperature prediction using Bayesian inference focuses on the temperature evolution in the subsurface at the location of the inactive BHE over five years, resulting from the operation of the four active BHEs. Temperatures are measured monthly with a spatial resolution of 1 m, up to a depth of 60 m. As this study focuses primarily on the investigation of temperature dynamics in the field, temperature changes are considered rather than absolute values. The subsurface of the field is characterized by its heterogeneity, consisting of three distinct layers, each with unique thermal properties. Each layer is assumed to be 20 m thick, and each BHE reaches a depth of 50 m.

The arrangement of the BHEs in the field is carefully designed to mitigate potential extreme thermal impacts on the surrounding environment. Therefore, the BHEs are spaced 10 m apart, adhering to recommendations from [49]. This spacing is particularly important in managing the thermal plume distribution, which is influenced by conductive heat transfer and advective mechanisms driven by groundwater flow.

Additionally, the variability in groundwater flow velocities among the different layers is considered, as it significantly affects the thermal conditions in the subsurface. As a result, the thermal state of each layer is closely tied to the prevailing hydrogeological conditions, with variations in groundwater velocity across the layers influencing the distribution and intensity of the generated thermal plume around the BHEs.

To achieve realistic thermal dynamics within this BHE field, temperatures and heat extraction rates in the layers are simulated using a numerical model developed in COMSOL Multiphysics® software. This numerical model represents the BHEs as double U-pipes, utilizing the Pipe Flow Module to simulate heat and fluid transfer within the pipes. The inactive BHE, which does not extract or inject heat, is solely dedicated to monitoring temperature variations through strategically placed sensors.

For the simulation, the inlet temperature and flow rates of the heat carrier fluid need to be specified. Each BHE is assigned a constant flow rate of 0.25 m s^{-1}, with an inlet fluid temperature set to 4 °C. The surface and the entire model domain are maintained at an undisturbed temperature of 12 °C, with all remaining model boundaries thermally insulated. The simulation domain encompasses an area of 400 m × 200 m × 100 m, divided into three subdomains to represent the geological layers. The numerical model is sufficiently sized to avoid unwanted effects from the model boundaries. A fine mesh with 1,073,656 elements ensures adequate resolution and accuracy.

The Heat Transfer in the Porous Media Module is employed to account for advective heat transfer, incorporating the material properties detailed in Table 1 and taken from [45]. By assuming a constant effective porosity, the groundwater flow velocity is proportional to the presented Darcy flow rate. The horizontal component of groundwater velocity in each layer is considered in the simulation. The study spans a simulation period of five years, with monthly monitoring of temperature changes along the observation points (inactive BHE) and the averaged heat extraction rates (active BHEs) from each geological layer for each month. This simulation period allows for a thorough analysis of the long-term thermal performance and the interaction between the BHEs and the surrounding subsurface.

Fig. 5 shows the simulated temperature changes along the depth profile over the entire time. These values are derived from the numerical model and serve as a reference for temperature changes in the inversion process.

The average heat extraction rate of all BHEs in each layer over the entire duration is presented in Fig. 6. These values, obtained from the numerical model, will be used exclusively to assess the efficiency of the inversion process of heat extraction rates.

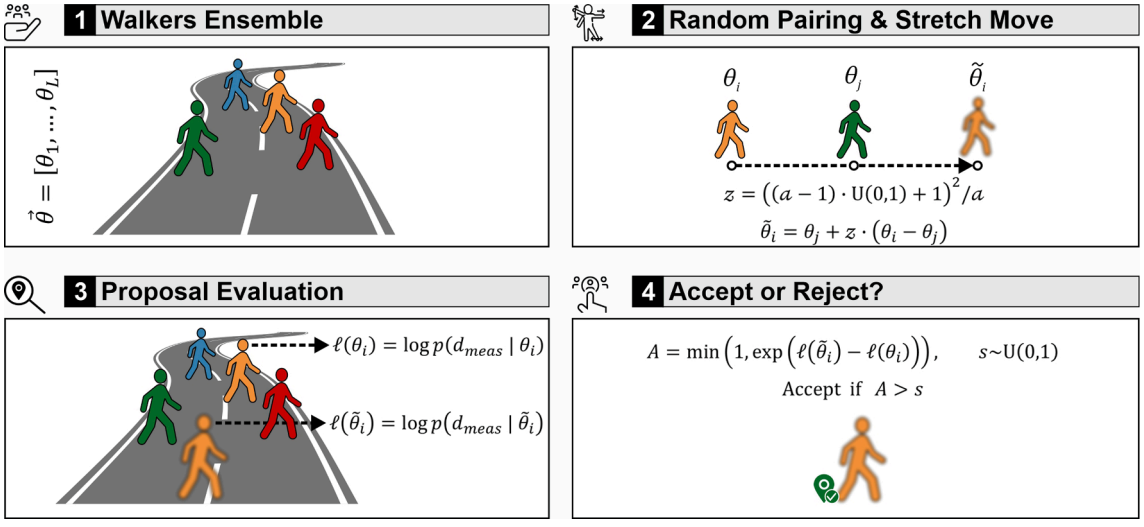


Fig. 3. Schematic illustration of the affine invariant ensemble MCMC sampler strategy for proposing new model samples.

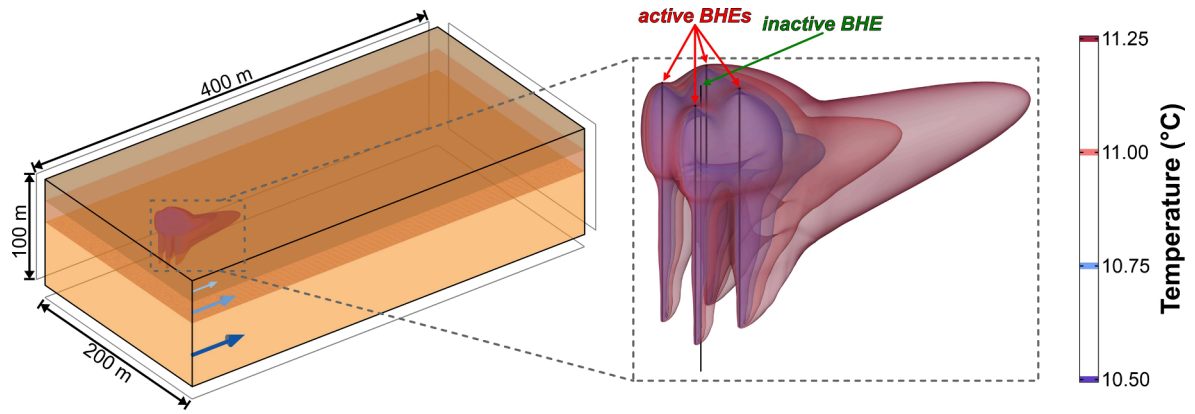


Fig. 4. Three-dimensional view of the numerical model with three layers and groundwater flow in COMSOL (left) and the configuration of BHEs in the field showing the thermal plume after five years of operation (right).

Table 1
Reference model parameters for different layers.

Parameters	Layer 1	Layer 2	Layer 3
$\lambda_m (\mathrm{Wm^{-1}K^{-1}})$	1.5	2	2.5
$u_x (\mathrm{ms^{-1}})$	1×10^{-7}	1×10^{-6}	3×10^{-6}
$\rho_m (\mathrm{kgm^{-3}})$	1600	2000	2000
$c_m (\mathrm{Jkg^{-1}K^{-1}})$	1200	1300	1500
ϕ	0.26	0.26	0.26

As illustrated in Fig. 6, the heat exchange rate in the BHE field is primarily influenced by the subsurface properties and hydrogeological conditions of the first two geological layers, as the BHEs are 50 m deep.

In layer 1 (0–20 m), heat transfer is dominated by conduction due to the very low groundwater velocity and moderate thermal conductivity. As a result, the thermal anomaly forms around the BHEs and gradually spreads outward over time. This slower heat dissipation means the heat exchange and thermal evolution will take longer to reach steady-state conditions in this layer.

In layer 2 (20–40 m), heat exchange is more efficient because of higher thermal conductivity and a moderate groundwater flow rate, which facilitates both conduction and convection. The increased groundwater flow carries heat away more effectively, allowing the system to reach steady-state conditions faster in this layer compared to layer 1.

Layer 3 (40–60 m), beyond the full reach of the BHEs, has minimal impact on heat transfer, although heat diffuses into it over time. Layer 3 has the highest groundwater velocity and thermal conductivity and it does not fully interact with the BHEs, limiting its effect on heat exchange. As a result, steady-state conditions in this layer are reached faster than in the others, which has a minor influence on the overall heat exchange performance.

In the following sections, the synthetic operational scenario simulated by the numerical model will be used to showcase the application of the proposed Bayesian procedure. It is important to note that the numerical model and its results are not part of the proposed Bayesian framework; they are solely used to demonstrate how the procedure works. In practice, the COMSOL model results should be replaced with field data measurements. The effectiveness of the Bayesian inversion procedure in modeling and predicting the subsurface temperature changes depends on the suitability of the forward model in accurately describing the underlying physical processes.

To model temperature changes around the BHEs in a multi-layered subsurface with groundwater flow, the well-established, computationally efficient MFLSA is employed, as discussed in Section 2.1. This analytical model captures the key physics involved, ensuring the reliability of the Bayesian inversion results. Although the numerical setup developed in this section serves only as a synthetic case for measured temperatures in the field to demonstrate the proposed approach and does not require validation, it is useful to ensure that associated uncertainties in the inversion procedure are not caused by unexplained variability in temperature changes due to the modeling tools. To address this, the numerical setup is validated against the MFLSA using reference model parameter values at selected timesteps, as shown in Fig. 7. The MFLSA analytically simulates temperature changes at these timesteps,

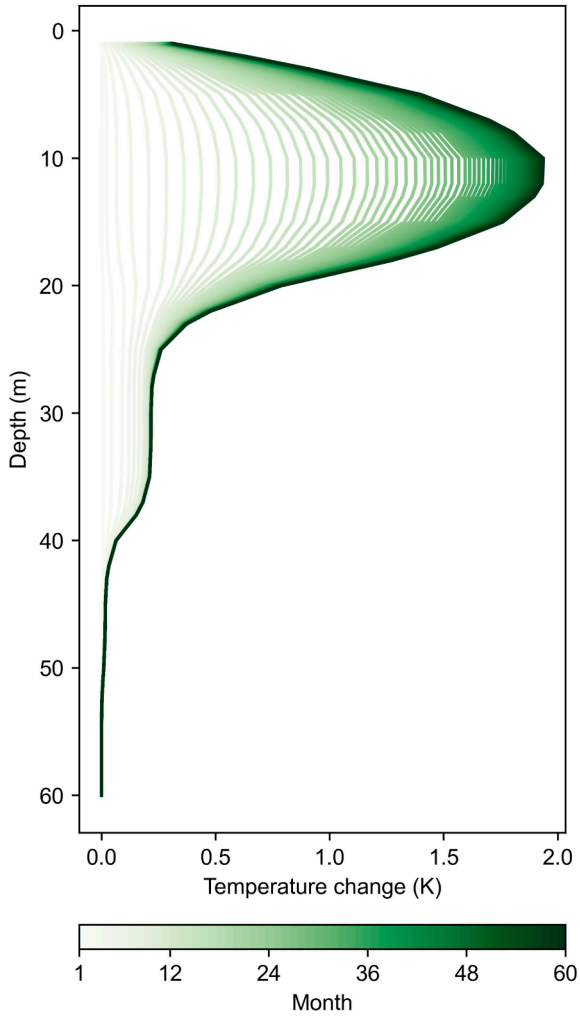


Fig. 5. Reference monthly temperature changes along the depth, simulated by the numerical model.

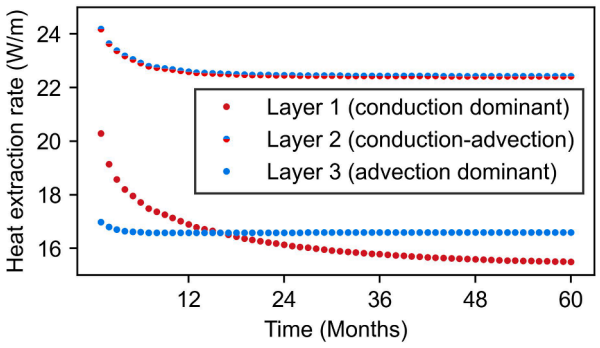


Fig. 6. Reference average heat extraction rate of BHEs in different layers, simulated by the numerical model.

assuming that temperature changes from earlier timesteps are measured and known. The results indicate that the MFLSA predictions closely align with the numerical model, confirming two key points: first, the forward model can accurately represent the numerical setup in this case, and second, the uncertainties of interest, which will be discussed in later sections, are not due to the inherent reliability of either the numerical or analytical model.

2.4. Implementation of the inversion procedure

This section details the specific settings of the inversion problem for the introduced BHE field. The goal of the inversion process is to determine the distribution of three unknown parameters — heat extraction rate (q), thermal conductivity (λ), and Darcy velocity (u) — across three layers, resulting in an inverse problem with nine unknown parameters over 60 timesteps.

For each unknown parameter, a uniform prior distribution within a specified range $[\alpha \ \ \beta]$ is assumed, reflecting the absence of strong prior information:

$$p(\theta) = \begin{cases} \dfrac{1}{\beta - \alpha}, & \text{if } \alpha \le \theta \le \beta \\ 0, & \text{otherwise} \end{cases} \tag{20}$$

The choice of this prior ensures that all values within the range $[\alpha \ \ \beta]$ are equally likely before considering the observed data, thereby allowing the data to primarily drive the inversion process.

Specifically, the ranges for the parameters are as follows: heat extraction rate ranges from 5 to 40 $\mathrm{W\,m^{-1}}$, thermal conductivity ranges from 0.5 to 4 $\mathrm{W\,m^{-1}K^{-1}}$, and Darcy velocity can vary from 6×10^{-8} to 6×10^{-6} $\mathrm{m\,s^{-1}}$.

The variance of the likelihood function in each timestep is derived from the error between simulated and observed temperature changes in the previous timestep.

For the implementation of the AIES, similar to the "walk move" formulation in [50], the density function is simulated using a transformed uniform distribution. However, unlike the "walk move" which is not affine invariant, the "stretch move" applied by the AIES formulation ensures affine invariance [51]:

$$z = ((a - 1)\cdot \mathrm{U}(0,1) + 1)^2 / a \tag{21}$$

Here a is the step size and is set to 2 in our study and U is a uniform distribution between 0 and 1.

In this study, the MATLAB implementation of the AIES by [51] is used. In each timestep 50,000 iterations and 180 walkers are employed to generate 5,040 samples for each unknown parameter.

The temperature changes shown in Fig. 5 are assumed to be the actual measurements, with the MFLSA being used in the forward solver for predicting temperature changes. At the end of each timestep, the median of all samples for each parameter is considered as the inferred model parameter for the simulation of the upcoming months. Additionally, simulated temperature change values of the current month are replaced by measured data as they become available. The process involves superimposing the current measured temperatures onto the predictions for future timesteps.

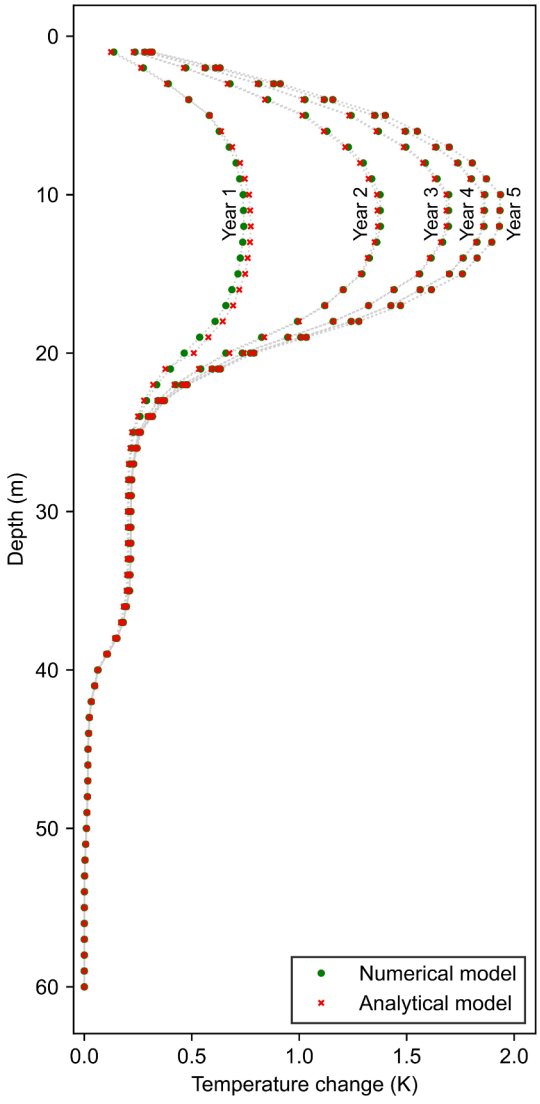


Fig. 7. Validation of the numerical results against the forward model at five timesteps, using reference input values and assuming known temperature changes from earlier timesteps.

3. Results and discussion

3.1. Statistical analysis of MCMC sampling

In this section, the performance of MCMC sampling with the affine invariant ensemble sampler (AIES) algorithm is evaluated. The purpose of this analysis is to determine whether the sampling process effectively explores the target distribution and has reached convergence—a state where the sampled values stabilize around the target distribution.

To assess convergence and sampling efficiency, trace plots are used, which display the progression of the parameter estimation. Trace plots help to reveal whether the "walkers" (or model samples) are thoroughly exploring the range of possible parameter values or, conversely, are becoming confined to certain areas. Effective sampling should ideally result in a trace plot where the walkers exhibit a random, well-

distributed pattern, covering the parameter space without showing a clear trend. In this study, trace plots are examined at five selected timesteps for nine unknown model parameters, including heat extraction rate (q), thermal conductivity (λ), and Darcy velocity (u) across three different layers. For clarity, only every tenth sample is shown in Fig. 8. The mean of all samples is also analyzed, and an overall trend is identified using linear regression to capture any underlying patterns. The trace plots reveal an erratic pattern, indicating that the walkers are "well-mixed", i.e., they move freely across the parameter space without becoming confined to specific regions. This pattern suggests effective exploration of the target distribution [47].

Most parameters in the trace plots exhibit stable, consistent patterns over time, with no discernible trends, suggesting that the samples have reached convergence, meaning they center around the target distribution. However, two exceptions occur: in the sixth month, thermal conductivity in the first layer displays a slight decreasing trend, while

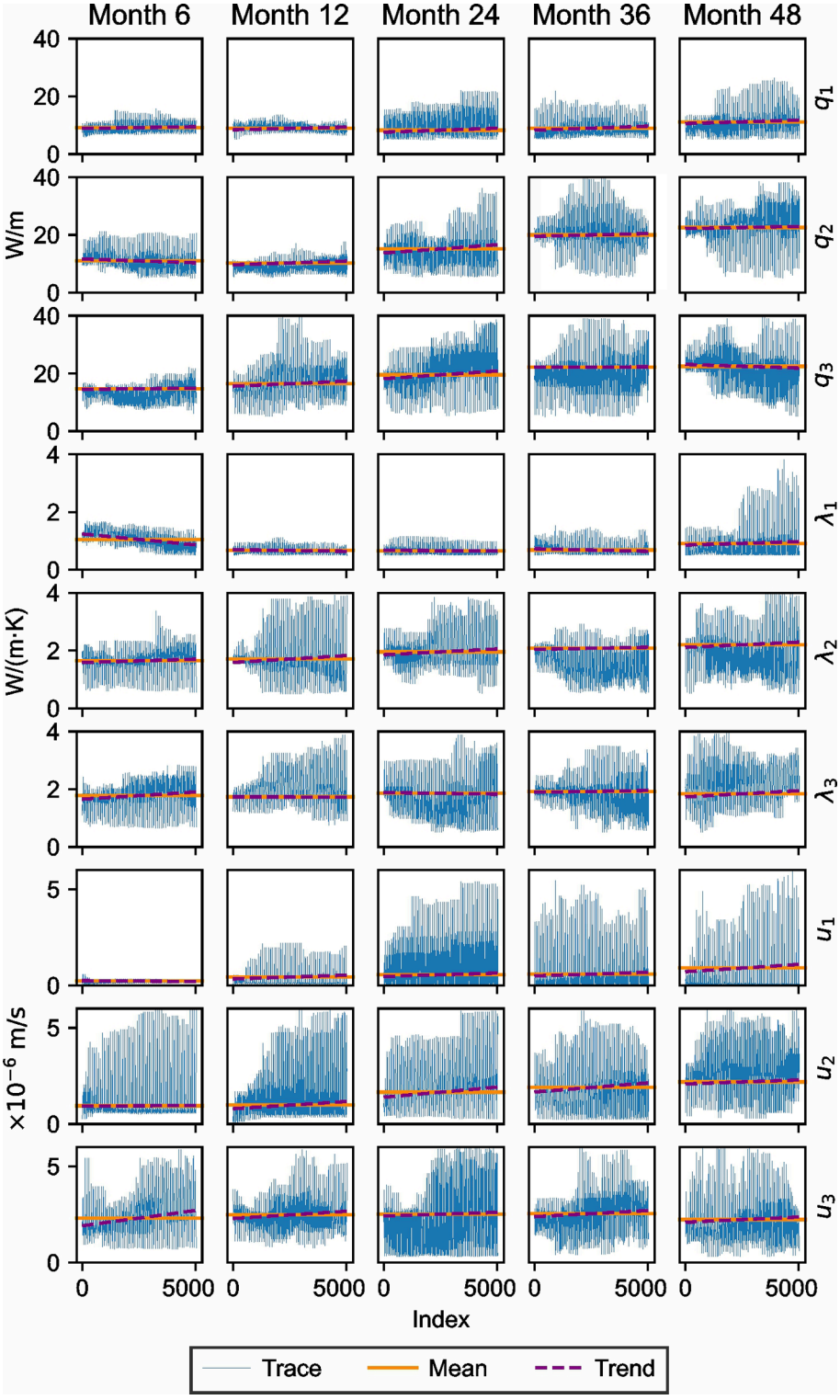


Fig. 8. Trace plots of model samples for nine parameters (heat extraction rate (q), thermal conductivity (λ), and Darcy velocity (u) for three layers) at five different timesteps.

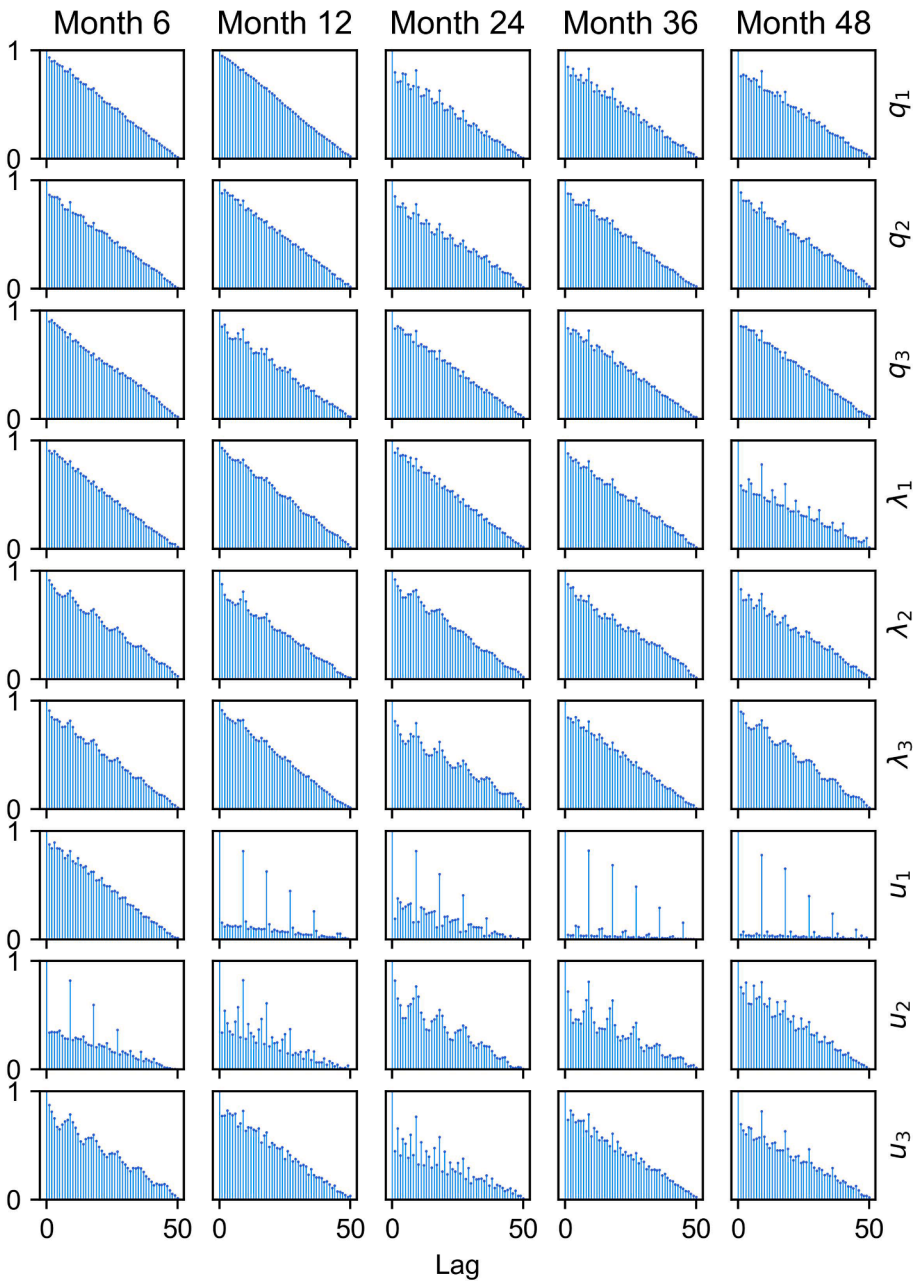


Fig. 9. Autocorrelation of the nine model parameters (heat extraction rate (q), thermal conductivity (λ), and Darcy velocity (u) for three layers) at five different timesteps, up to a lag of 50.

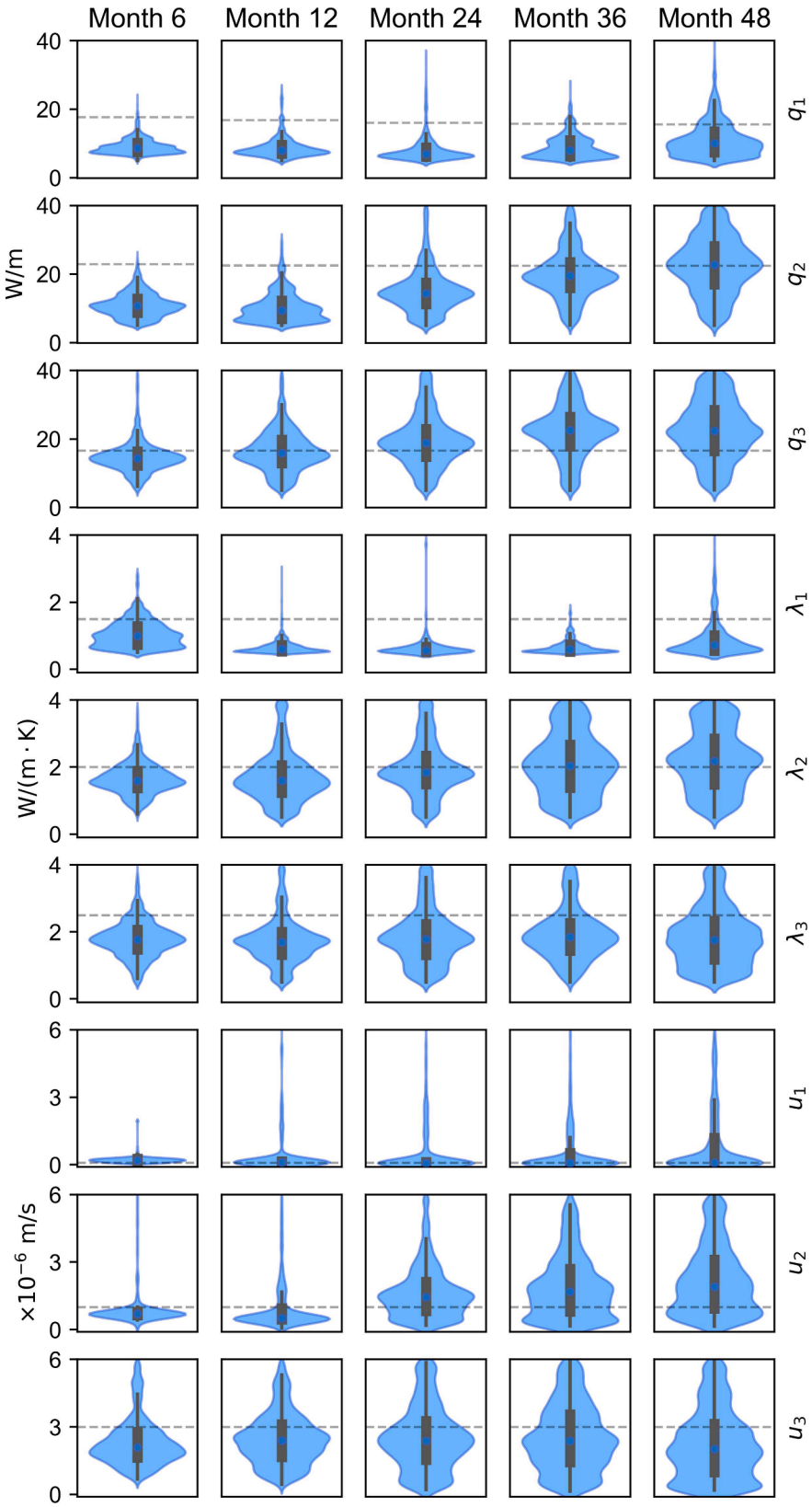


Fig. 10. Violin plots of the nine model parameters (heat extraction rate (q), thermal conductivity (λ), and Darcy velocity (u) for three layers) at five different timesteps. The dashed line represents the reference value for each parameter.

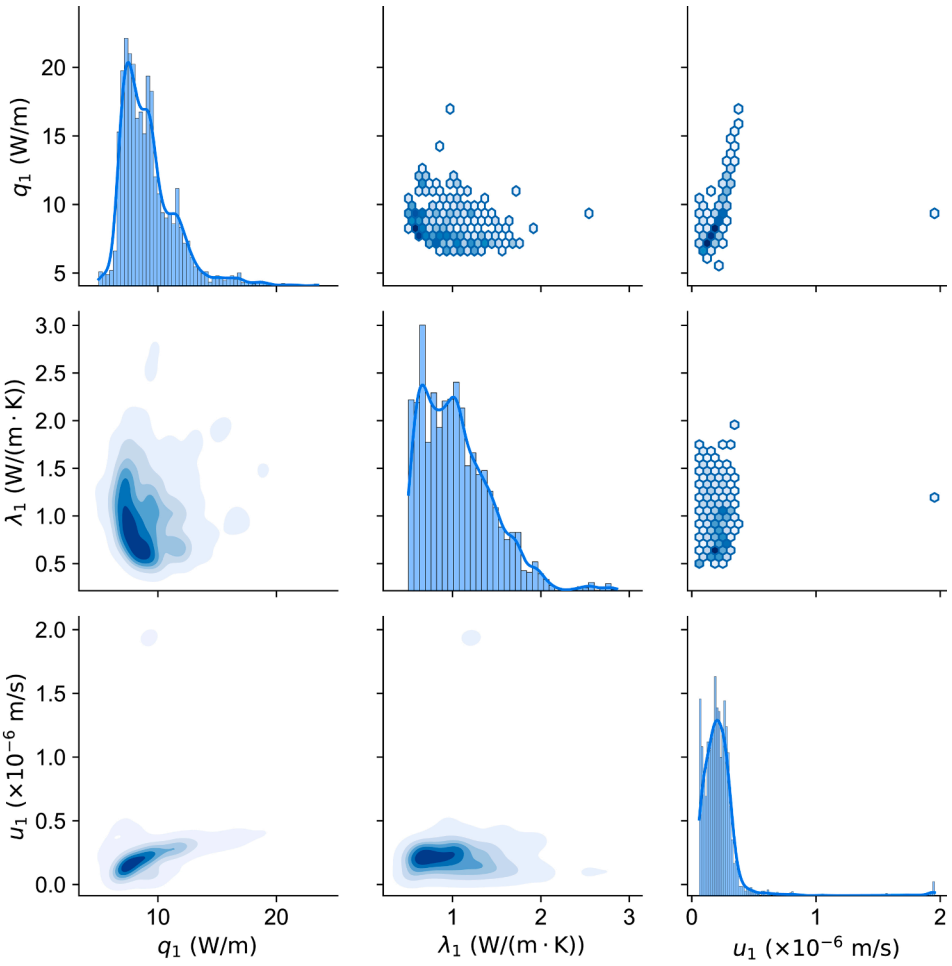


Fig. 11. Pair plots of heat extraction rate (q_1), thermal conductivity (λ_1), and Darcy velocity (u_1) within the first layer at month 6.

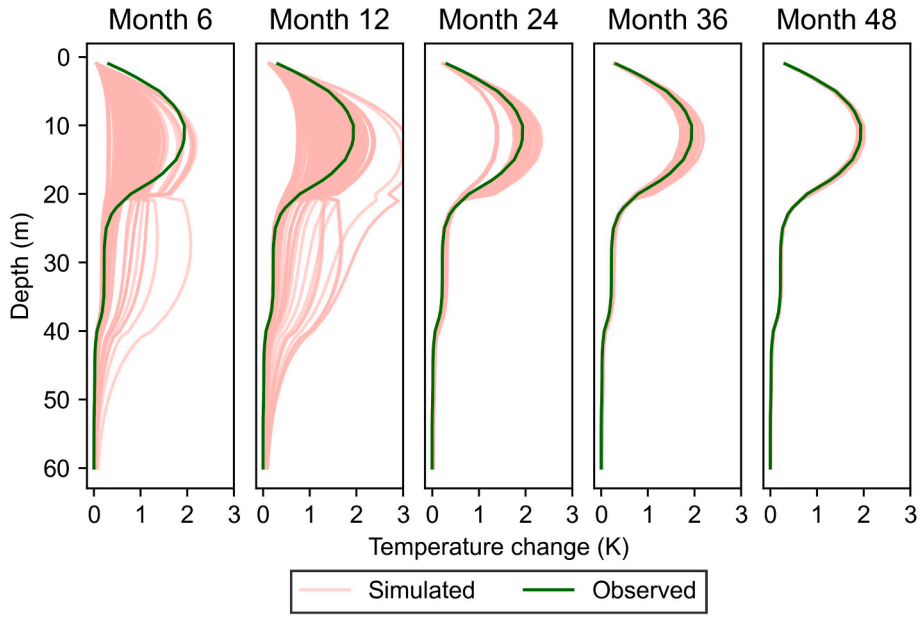


Fig. 12. Comparison of simulated and observed temperature changes at month 60 over the depth, using inferred model parameters from months 6, 12, 24, 36, and 48.

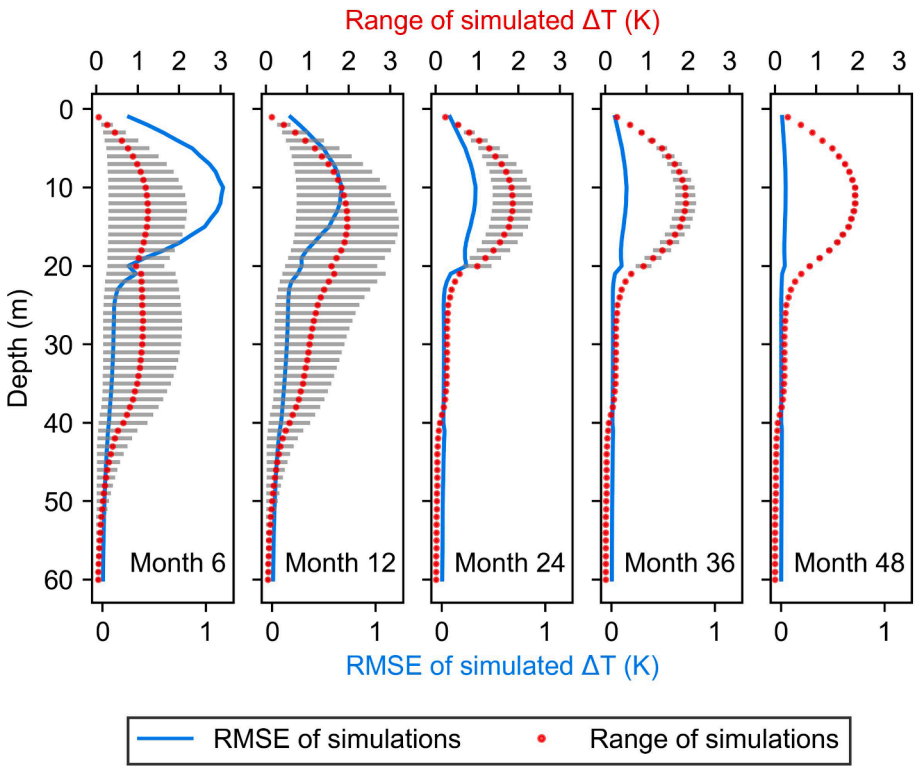


Fig. 13. Comparison of the root mean square error (RMSE) and the range of temperature change predictions at month 60, based on the model samples from months 6, 12, 24, 36, and 48.

groundwater velocity in the third layer shows an increasing trend. These trends do not persist in later timesteps, further supporting the finding that the walkers have reached the target distribution. Over time, the parameter values fluctuate around a consistent mean, indicating that the samples are in a stationary state with stabilized sampling behavior. It is also observed that the amplitude (range) of fluctuations, in the trace plots increases slightly over time, i.e., in the earlier timesteps, the samples exhibit a tighter range of values for the model parameters. This is because, in the early months, larger temperature changes better constrain the parameter estimation, narrowing the search radius within the plausible exploration space. In summary, this analysis shows that the sampling has achieved stationarity, consistently exploring the parameter space without exploration bias, in a well-mixed manner. In the next step, to assess whether the generation of each sample is independent of other samples, autocorrelation plots are employed (Fig. 9). Autocorrelation measures the similarity between the samples as a function of "lag", i.e. the number of iterations between samples. Constant high autocorrelation indicates that samples are too similar, suggesting poor mixing of the sampling methodology. Effective MCMC sampling should display decreasing autocorrelation with increasing lag, showing that samples become more independent as the gap between them grows [52].

In Fig. 9, autocorrelation is calculated for the samples of each model parameter at various timesteps, with a thinning factor of 100 and a maximum lag of 50. For most parameters, autocorrelation decreases as the lag increases, indicating that realized samples are relatively independent and that the walkers mix well. However, an exception is found in the Darcy velocity of the first layer (u_1), where repetitive spikes in autocorrelation appear at later time steps, indicating higher correlations between nearby samples. This pattern suggests that u_1 may have converged to its target distribution earlier, resulting in less variability in subsequent samples. This could indicate that the early temperature data strongly constrains this parameter, generating samples that consistently reflect the already determined target value. This implies a so-called high information content of the temperature data during early timesteps for the first layer.

3.2. *Evaluation of the posterior samples*

To gain a deeper understanding of the results from the MCMC sampling, violin plots are used to visualize the distributional characteristics of the generated model parameter samples (Fig. 10). These plots are particularly useful in this context, as they reveal the density and variability of the generated model samples. Fig. 10 illustrates this information for all parameters, using the same selected timesteps shown in the previous figures, providing a more comprehensive view of how the uncertainty in the model samples evolves. As shown in Fig. 10, the parameters in the first layer are more tightly distributed when compared to those in the other layers.

This narrower distribution in the first layer corresponds to earlier findings, which suggested that the thermal state in this layer, influenced by lower advection, leads to more significant temperature changes. These changes indicate high parameter sensitivity, which in turn helps to constrain the parameter space more strictly.

In the first layer, the samples for both thermal conductivity (λ_1) and Darcy velocity (u_1) are clustered around a single mode for most timesteps, indicating high certainty in the parameter estimates. This is particularly evident for Darcy velocity (u_1), where the statistical distribution is especially tight. This aligns with the autocorrelation analysis from Fig. 9, which showed that after a few months, the inference of groundwater flow rate in the first layer has stabilized. Therefore, further Bayesian investigations for this parameter would not be necessary and could be treated as a minimization problem instead. However, the strong correlations between parameters and interactions across layers still necessitate the use of the Bayesian framework to understand the relationships in the parameter space.

In contrast, the distributions of Darcy velocity samples in the second (u_2) and third (u_3) layers show greater variability. This can be attributed to the heat transfer dynamics in these layers, where slower thermal

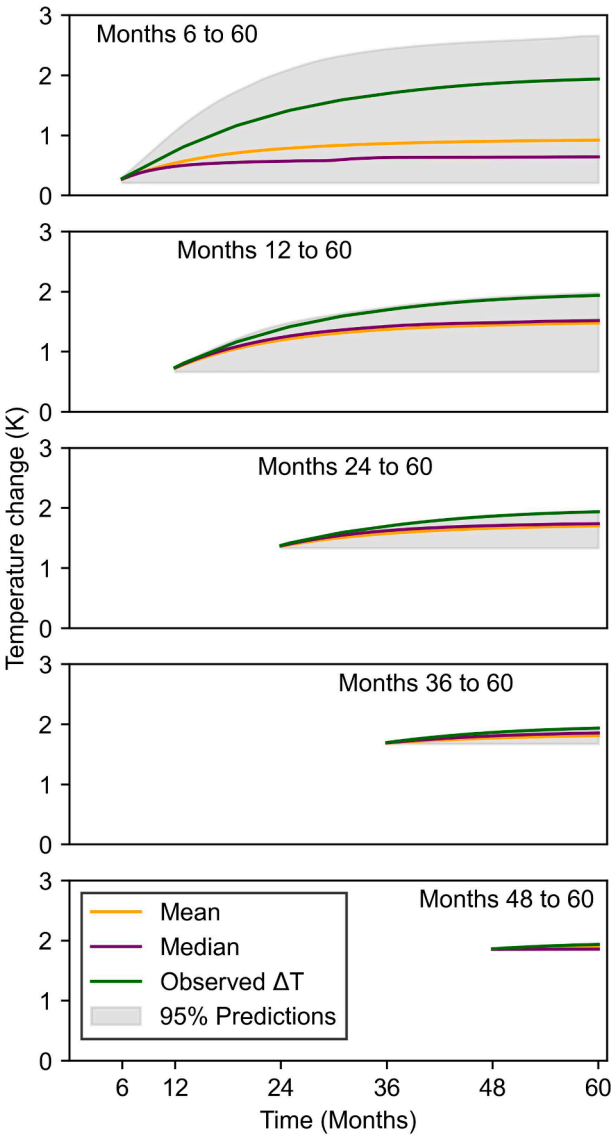


Fig. 14. Comparison of the 95 % confidence interval, mean, and median of predicted temperature changes with observed temperature changes at a depth of 10 m, using inferred parameters from months 6, 12, 24, 36, and 48 until the end of the operation.

changes in later timesteps lead to less pronounced temperature shifts. As a result, a wider range of groundwater flow rate values can explain the observed temperatures, leading to greater uncertainty in the parameters for these layers. The consistent findings that the parameters in the first layer exhibit the strongest correlations indicate that they are the most influential factors in determining temperature changes in the field. To further explore the relationships between pairs of model parameters, an analysis of the correlation between the heat extraction rate (q_1), thermal conductivity (λ_1), and Darcy velocity (u_1) in the first layer in the sixth month is performed. This analysis is illustrated in Fig. 11, where the lower left triangle of the figure displays contour plots, while the upper right triangle features hexbin plots. Each hexagon represents a minimum of 15 samples at that position in the parameter space, with darker colors indicating higher frequencies of samples. The diagonal subplots show histograms of sample distributions, along with the estimated kernel density distributions.

The histogram of correlations reveals a multimodal distribution for heat extraction rate and thermal conductivity, while a unimodal distribution is observed for Darcy velocity. Although all parameters are correlated at this timestep, the strongest correlation is between Darcy velocity and the heat extraction rate. For a more comprehensive analysis, the pair plots of all nine parameters at five different timesteps are presented in the Appendix. Notably, correlations are observed not only within individual layers but also between different layers over time. This observation aligns with the governing heat transfer in the domain. Initially, a significant temperature difference between the inlet fluid in the pipe and the surrounding environment can be assumed, leading to a higher expected heat exchange rate in the first layer at early times. Due to the higher temperature differences in the first layer, the fluid inside the pipe extracts a relatively large amount of energy from the ground. As a result, the heated fluid entering the second and third layers has a higher temperature, causing a decrease in the heat extraction rate in the first layer over time. However, higher advection in the second and third layers mitigates the cooling effect, maintaining a relatively constant heat extraction rate in those layers. This interaction between the layers can also be identified statistically in the pair plots of Fig. 11.

3.3. Simulated temperature changes

So far, the generated samples using various statistical analyses have been discussed. However, the primary goal of this work is not merely to infer parameters, but to improve the prediction of thermal states in the field. Therefore, this section focuses on predicting temperature changes around the BHE in a stochastic manner, utilizing the measured temperatures from the inactive BHE over the operation time. As a first scenario, five timesteps at months 6, 12, 24, 36, and 48 are selected and at the end of each timestep, the measured temperatures are used within the Bayesian framework to infer a set of model parameters. These inferred parameters are then directly applied to predict temperature changes in the field across the layers after five years of operation. The results of these predictions, with a thinning factor of ten applied to the samples, are shown in Fig. 12.

It is revealed that over time, as more information is gathered, the uncertainty in the predictions is significantly reduced. Initially, most of the generated samples for the parameters in the first layer tend to underestimate the temperature, but as time progresses, the proposals are chosen more efficiently. To better quantify the results shown in Fig. 12, the root mean square error (RMSE) for temperature change predictions at month 60 is plotted in Fig. 13. All sampled parameters from months 6, 12, 24, 36, and 48 are included in this analysis to predict the temperature change at the end of month 60 along the entire depth.

It is observed that the maximum RMSE for predictions using samples from month 6 is 1.17 K, which decreases to 0.05 K with the consideration of samples from month 48. Similarly, the maximum range of temperature change predictions reduces from 1.91 K to 0.16 K as the month progresses from 6 to 48. This indicates that uncertainty in the temperature predictions for the final timestep reduces to 8 % when inferred samples from month 48 are used. It should be noted that the faster dynamics of temperature change in the early months make capturing the correct behavior of temperature variation more challenging. However, if certain subsurface parameters, such as groundwater flow rate, or operational parameters, like the flow rate of the heat carrier fluid, change over time, fast temperature changes may also occur even in the later timesteps.

As expected from the statistical analysis, the first layer, due to low groundwater velocity and local cooling, is the main source of uncertainty for predicting temperatures. It is observed that predictions from layers 2 and 3 are more accurate, as they can more rapidly approach the true thermal state. This is because temperature signals in these layers reach a steady state more quickly, leading to smaller variations between timesteps. In the first case, the spatial predictability of the proposals across the entire depth is analyzed. As a further analysis, an examination of temperature changes within the first layer over entire timesteps is conducted. Therefore, the same five timesteps (months 6, 12, 24, 36, and 48) are selected, and based on the inferred parameters at each timestep, the simulated temperature change until the end of the operation is compared. The temperature change at a depth of 10 m is presented in Fig. 14.

This result clearly shows a reduction in temperature uncertainty over time. Similar to the previous case, predictions based on early inferred parameters cannot accurately reproduce the transient temperature evolution and tend to predict an earlier steady state for the subsurface system. For instance, by comparing the mean and median of predicted temperatures based on parameters from months 6 and 12, it is evident that predictions based on parameters from month 12 better follow the nonlinear transition from the transient phase to a quasi-steady state condition.

4. Conclusions

This study presents a probabilistic modeling framework for predicting long-term temperature changes in the subsurface surrounding borehole heat exchanger (BHE) fields, accounting for multi-layer subsurface heterogeneity and groundwater flow. Leveraging a Bayesian approach, the newly developed framework infers the high-dimensional, correlated parameter space essential for accurately modeling heat transport in the subsurface caused by the operation of BHEs in fields with complex geological settings. To achieve this, the affine invariant ensemble sampler within a stochastic Bayesian method characterizes nine correlated parameters—such as heat extraction rate, thermal conductivity, and Darcy velocity—across three distinct subsurface layers. An efficient analytical forward solver, the moving finite line source model with anisotropy (MFLSA) further enhances the framework's capacity to incorporate anisotropic conditions and groundwater flow.

To demonstrate the framework's applicability, a synthetic five-year case study is conducted in COMSOL Multiphysics®, involving four active BHEs and one inactive BHE. Monthly simulated temperatures obtained at the inactive BHE by the numerical model are used as reference data for parameter estimation and to evaluate the framework's temperature change predictions. Comprehensive statistical analyses confirm the successful characterization of the parameter space, thereby achieving reliable spatial and temporal temperature predictions. Sequential application of the framework over 32 months shows a reduction in prediction uncertainty to 8 % by the end of the five-year operation, underscoring the framework's effectiveness in managing long-term temperature predictions. However, the reduction in uncertainty may be less pronounced if operational conditions vary significantly over time.

Additionally, this framework extends the applicability of the MFLSA analytical model for realistic, heterogeneous subsurface scenarios by eliminating the need for a constant heat extraction rate across layers.

Future work will focus on applying this framework to real field data with extended, high-resolution measurements and exploring transient boundary conditions and variable operational parameters. Incorporating machine learning methods to further improve sampling efficiency, along with complementary data sources such as hydrogeological measurements and geophysical investigations, could refine the inversion process and enhance the reliability of inferred parameters.

CRediT authorship contribution statement

Hesam Soltan Mohammadi: Conceptualization, Data curation, Formal analysis, Investigation, Methodology, Software, Validation, Visualization, Writing – original draft, Writing – review & editing. **Lisa Maria Ringel:** Conceptualization, Investigation, Methodology, Validation, Writing – review & editing. **Christoph Bott:** Investigation, Software, Visualization, Writing – review & editing. **Selçuk Erol:** Methodology, Software, Writing – review & editing. **Peter Bayer:** Conceptualization, Funding acquisition, Methodology, Resources, Project administration, Supervision, Writing – review & editing.

Declaration of competing interest

The authors declare that they have no known competing financial interests or personal relationships that could have appeared to influence the work reported in this paper.

Acknowledgments

This work was supported by the German Research Foundation (DFG) based on grant number BA2850/7-1, and by the Federal Ministry for Economic Affairs and Climate Action of Germany (BMWK) based on grant number 03EE4039A, within the GEOTHERMICA project RECOIN (ID: 455). The authors thank Ryan Pearson, Wiebke Lehmann, and Lukas Römhild for proofreading. The authors also appreciate the constructive comments from the six anonymous reviewers that helped to improve the manuscript.

Appendix

Validation of the forward solver over depth and time (30 years), using data and results from [45] for the (hydro)geological settings provided in Table 1.

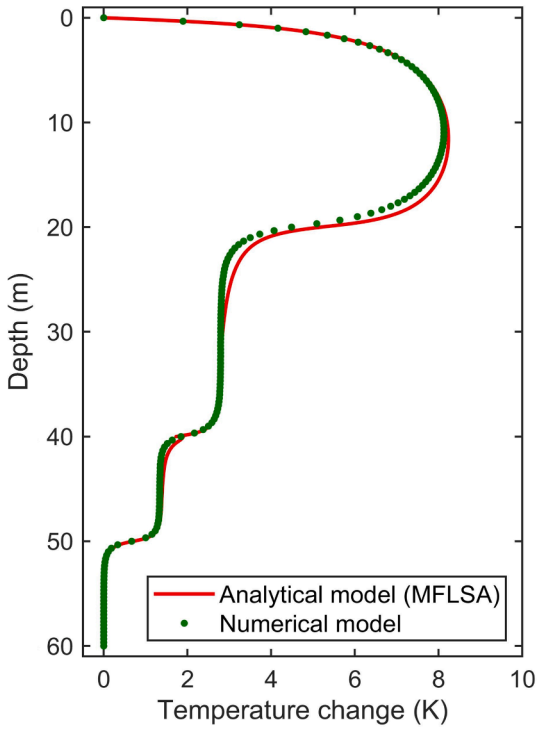


Fig. A1. Validation of the forward solver (MFLSA) with numerical results over depth.

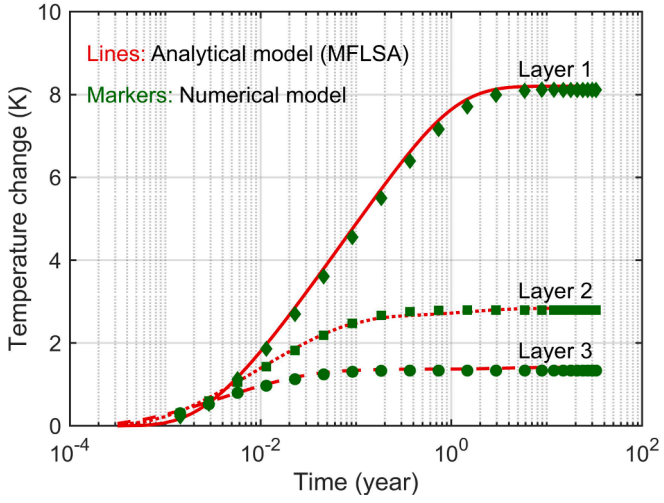


Fig. A2. Validation of the forward solver (MFLSA) with numerical results over time.

Pair plots for all nine parameters at different timesteps:

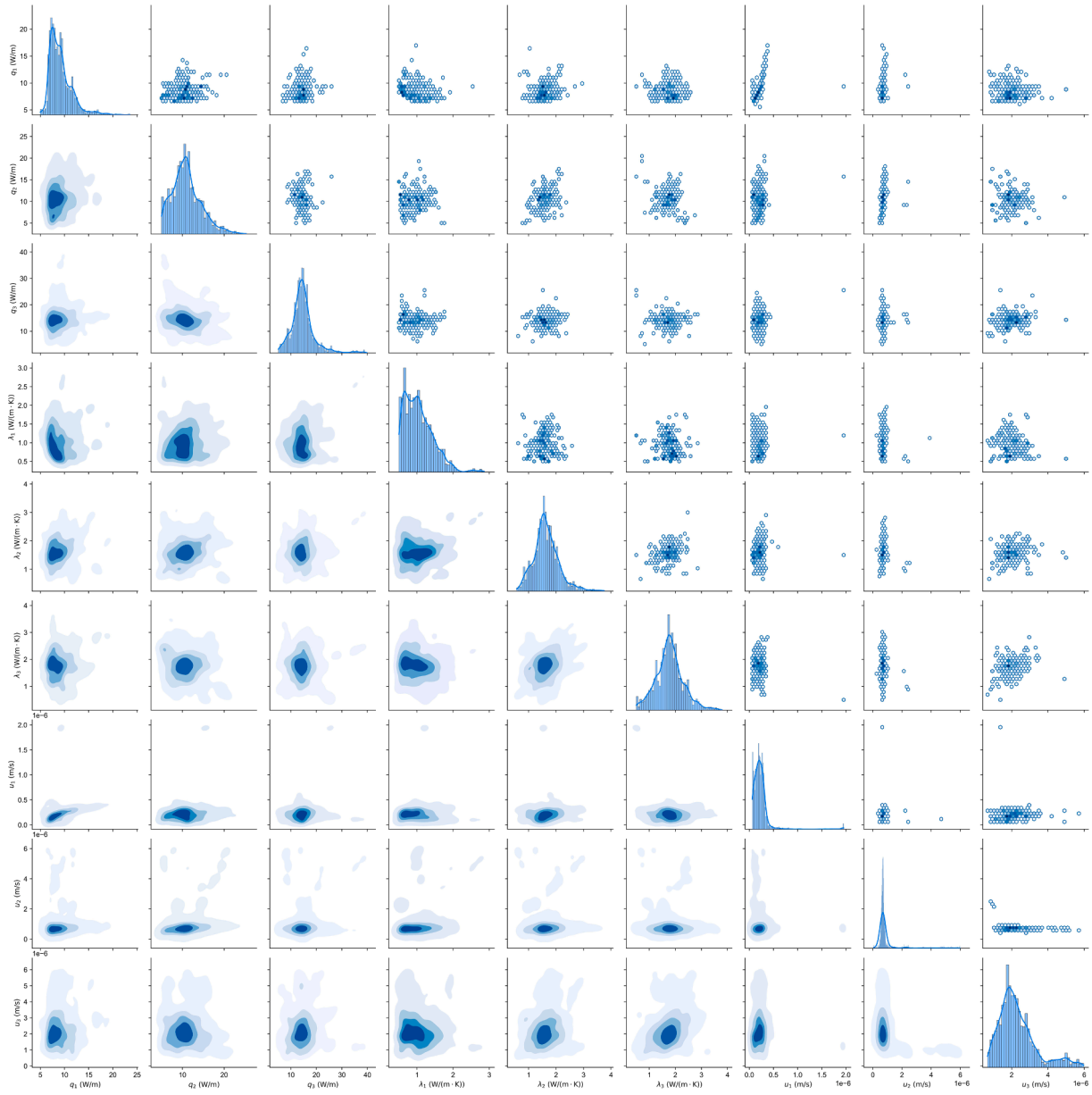


Fig. A3. Pair plots of all nine parameters at month 6.

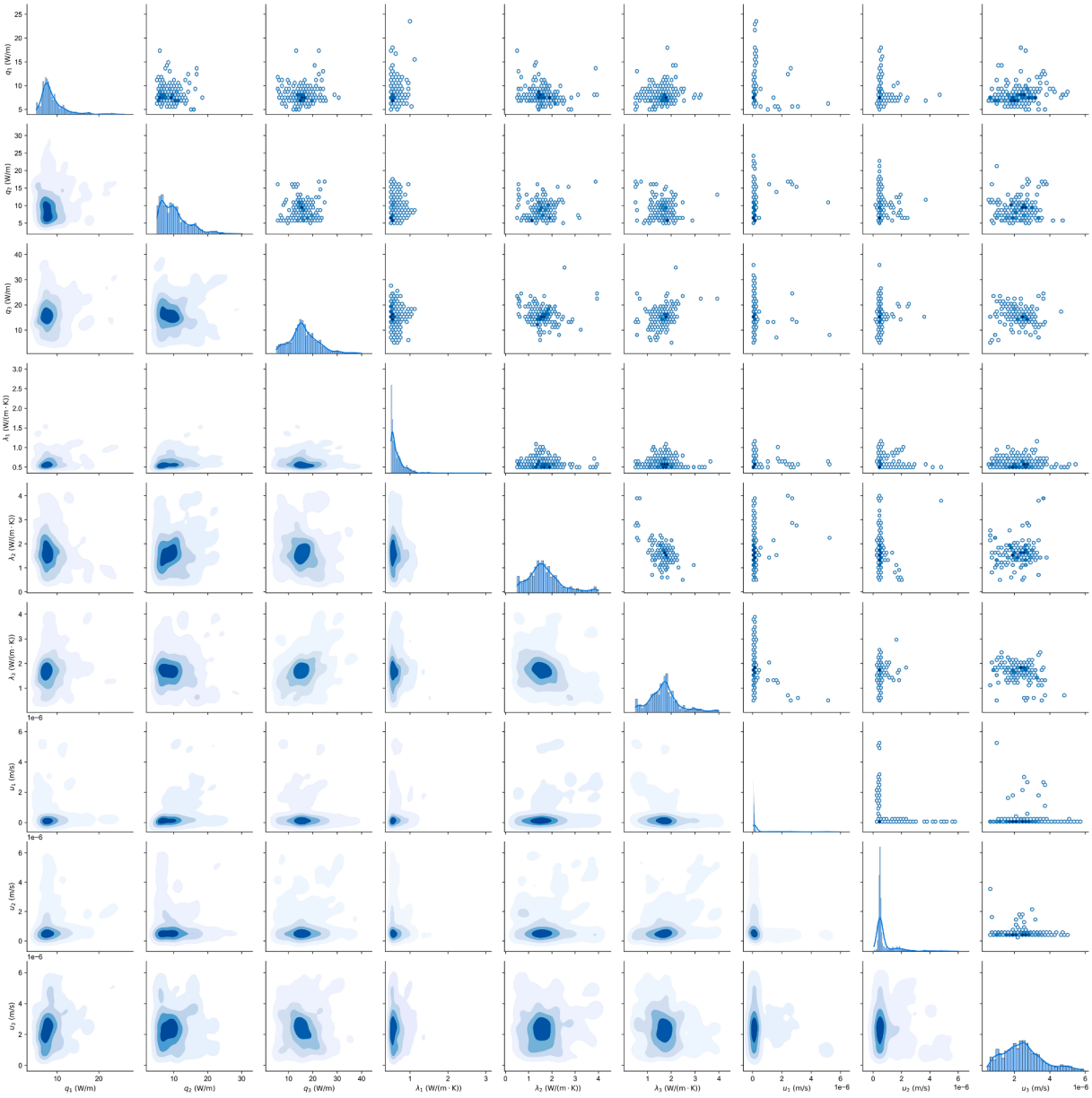


Fig. A4. Pair plots of all nine parameters at month 12.

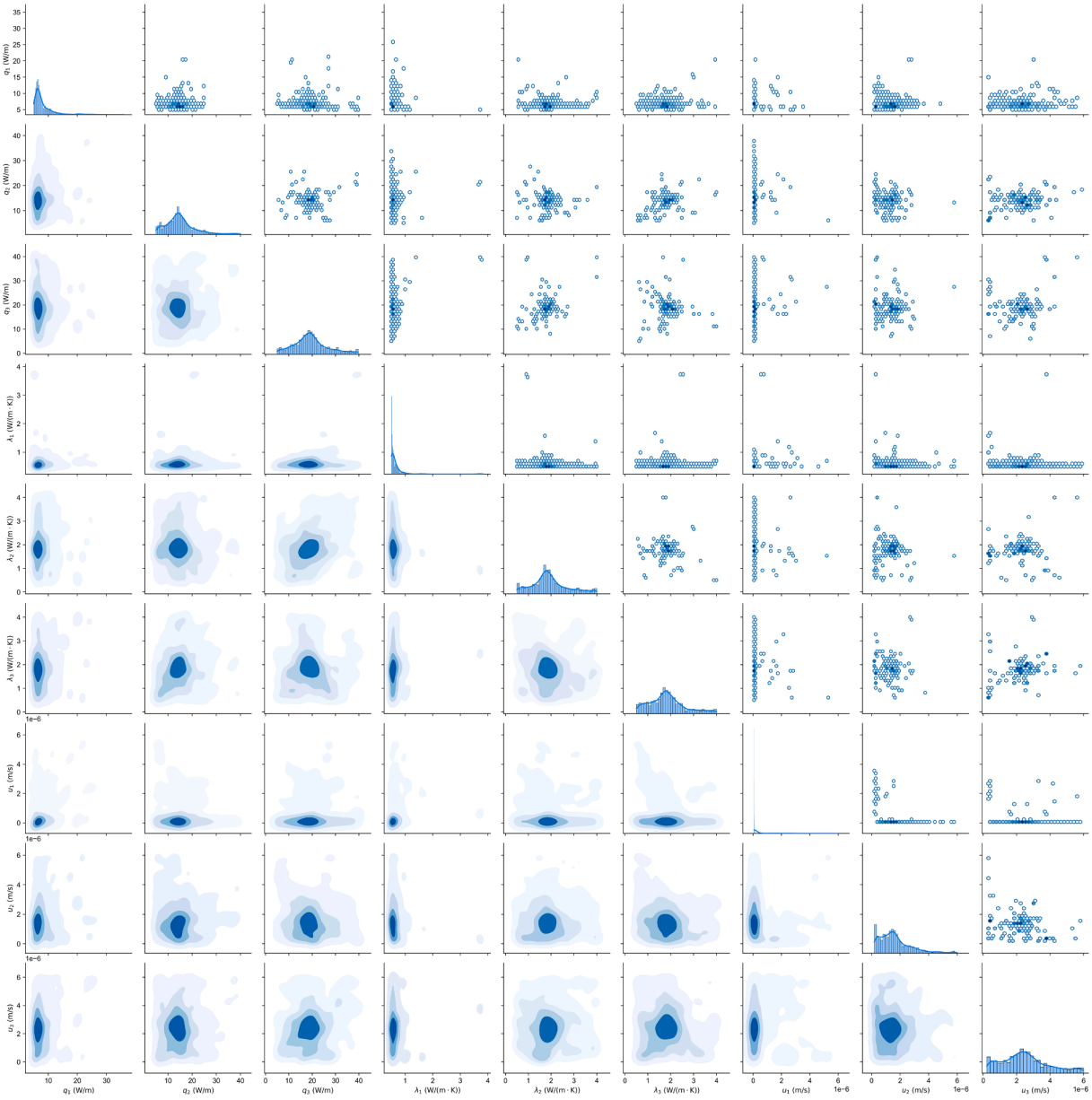


Fig. A5. Pair plots of all nine parameters at month 24.

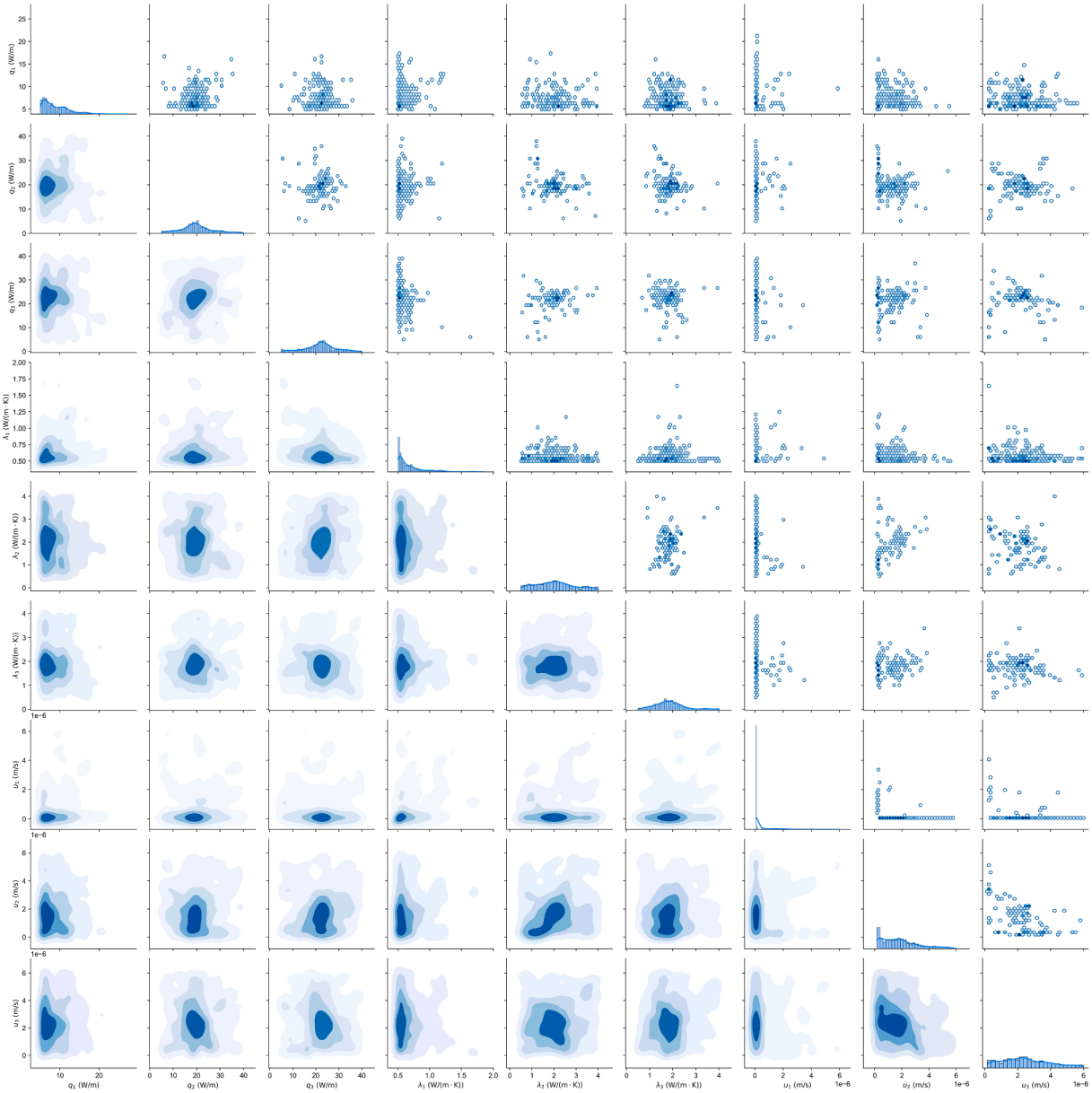


Fig. A6. Pair plots of all nine parameters at month 36.

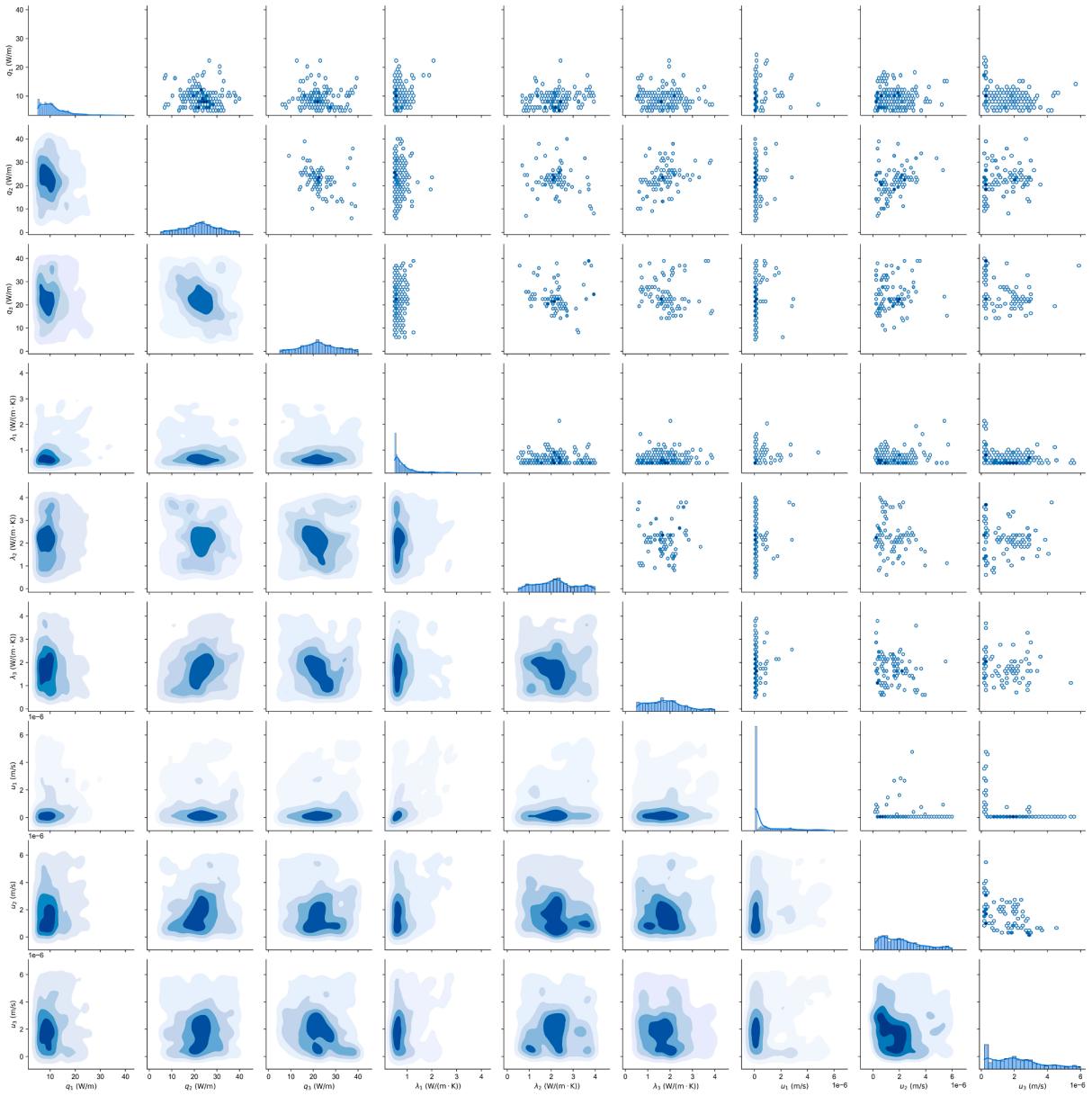


Fig. A7. Pair plots of all nine parameters at month 48.

Data availability

Data will be made available on request.

References

[1] S.A. Benz, K. Menberg, P. Bayer, B.L. Kurylyk, Shallow subsurface heat recycling is a sustainable global space heating alternative, Nat. Commun. 13 (2022) 3962.

[2] A.G. Gil, E.A.G. Schneider, M.M. Moreno, J.C.S. Cerezal, Shallow Geothermal Energy: Theory and Application, Springer Nature, 2022.

[3] F. Stauffer, P. Bayer, P. Blum, N.M. Giraldo, W. Kinzelbach, Thermal Use of Shallow Groundwater, CRC Press, 2013.

[4] S. Chen, W. Cai, F. Witte, X. Wang, F. Wang, O. Kolditz, et al., Long-term thermal imbalance in large borehole heat exchangers array – A numerical study based on the Leicester project, Energ. Buildings 231 (2021) 110518, https://doi.org/10.1016/j.enbuild.2020.110518.

[5] S. Haehnlein, P. Bayer, P. Blum, International legal status of the use of shallow geothermal energy, Renew. Sustain. Energy Rev. 14 (2010) 2611–2625.

[6] K.P. Tsagarakis, L. Efthymiou, A. Michopoulos, A. Mavragani, A.S. Anđelković, F. Antolini, et al., A review of the legal framework in shallow geothermal energy in selected European countries: Need for guidelines, Renew. Energy 147 (2020) 2556–2571, https://doi.org/10.1016/j.renene.2018.10.007.

[7] J.A. Rivera, P. Blum, P. Bayer, Increased ground temperatures in urban areas: Estimation of the technical geothermal potential, Renew. Energy 103 (2017) 388–400.

[8] P. Bayer, G. Attard, P. Blum, K. Menberg, The geothermal potential of cities, Renew. Sustain. Energy Rev. 106 (2019) 17–30.

[9] P. Blum, K. Menberg, F. Koch, S.A. Benz, C. Tissen, H. Hemmerle, et al., Is thermal use of groundwater a pollution? J. Contam. Hydrol. 239 (2021) 103791 https://doi.org/10.1016/j.jconhyd.2021.103791.

[10] M. Li, A.C.K. Lai, Review of analytical models for heat transfer by vertical ground heat exchangers (GHEs): A perspective of time and space scales, Appl. Energy 151 (2015) 178–191.

[11] Y. Guo, G. Huang, W.V. Liu, A new semi-analytical solution addressing varying heat transfer rates for U-shaped vertical borehole heat exchangers in multilayered ground, Energy 274 (2023) 127373.

[12] N. Molina-Giraldo, P. Blum, K. Zhu, P. Bayer, Z. Fang, A moving finite line source model to simulate borehole heat exchangers with groundwater advection, Int. J. Therm. Sci. 50 (2011) 2506–2513, https://doi.org/10.1016/j.ijthermalsci.2011.06.012.

[13] J.A. Rivera, P. Blum, P. Bayer, Analytical simulation of groundwater flow and land surface effects on thermal plumes of borehole heat exchangers, Appl. Energy 146 (2015) 421–433.
[14] Y. Guo, J. Zhao, W.V. Liu, A novel solution for vertical borehole heat exchangers in multilayered ground with Robin boundary condition, Appl. Therm. Eng. 123923 (2024).
[15] T. Coen, B. François, P. Gerard, Analytical solution for multi-borehole heat exchangers field including discontinuous and heterogeneous heat loads, Energy Build 253 (2021) 111520.
[16] R. Al-Khoury, Computational modeling of shallow geothermal systems, CRC Press, 2011.
[17] G.A. Florides, P. Christodoulides, P. Pouloupatis, Single and double U-tube ground heat exchangers in multiple-layer substrates, Appl. Energy 102 (2013) 364–373.
[18] H. Biglarian, M. Abbaspour, M.H. Saidi, A numerical model for transient simulation of borehole heat exchangers, Renew. Energy 104 (2017) 224–237, https://doi.org/10.1016/j.renene.2016.12.010.
[19] M.H. Jahangir, H. Sarrafha, A. Kasaeian, Numerical modeling of energy transfer in underground borehole heat exchanger within unsaturated soil, Appl. Therm. Eng. 132 (2018) 697–707, https://doi.org/10.1016/j.applthermaleng.2018.01.020.
[20] X. Yu, H. Li, S. Yao, V. Nielsen, A. Heller, Development of an efficient numerical model and analysis of heat transfer performance for borehole heat exchanger, Renew. Energy 152 (2020) 189–197, https://doi.org/10.1016/j.renene.2020.01.044.
[21] E. Dube Kerme, A.S. Fung, Transient heat transfer simulation, analysis and thermal performance study of double U-tube borehole heat exchanger based on numerical heat transfer model, Appl. Therm. Eng. 173 (2020) 115189, https://doi.org/10.1016/j.applthermaleng.2020.115189.
[22] A.L. Brettschneider, L. Perković, Theoretical analysis of using multiple borehole heat exchangers for production of heating and cooling energy in shallow geothermal reservoirs with underground water flow, Appl. Therm. Eng. 254 (2024) 123914, https://doi.org/10.1016/j.applthermaleng.2024.123914.
[23] S. Huang, J. Li, H. Gao, J. Dong, Y. Jiang, Thermal performance of medium-deep U-type borehole heat exchanger based on a novel numerical model considering groundwater seepage, Renew. Energy 222 (2024) 119988, https://doi.org/10.1016/j.renene.2024.119988.
[24] H. Soltan Mohammadi, L.M. Ringel, M. de Paly, P. Bayer, Sequential long-term optimization of shallow geothermal systems under descriptive uncertainty and dynamic variation of heating demand, Geothermics 121 (2024) 103021, https://doi.org/10.1016/j.geothermics.2024.103021.
[25] E. Heim, P. Stoffel, S. Düber, D. Knapp, A. Kümpel, D. Müller, et al., Comparison of simulation tools for optimizing borehole heat exchanger field operation, Geotherm. Energy 12 (2024) 24.
[26] S. Gehlin, Thermal response test: method development and evaluation, 2002.
[27] J.D. Spitler, S.E.A. Gehlin, Thermal response testing for ground source heat pump systems - An historical review, Renew. Sustain. Energy Rev. 50 (2015) 1125–1137, https://doi.org/10.1016/j.rser.2015.05.061.
[28] E. Heim, M. Laska, R. Becker, N. Klitzsch, Estimating the subsurface thermal conductivity and its uncertainty for shallow geothermal energy use—a workflow and geoportal based on publicly available data, Energies 15 (2022) 3687.
[29] G. Dion, P. Pasquier, D. Marcotte, Deconvolution of experimental thermal response test data to recover short-term g-function, Geothermics 100 (2022) 102302.
[30] G. Dion, P. Pasquier, D. Marcotte, G. Beaudry, Multi-deconvolution in non-stationary conditions applied to experimental thermal response test analysis to obtain short-term transfer functions, Sci. Technol. Built Environ. 30 (2024) 220–233.
[31] G. Dion, P. Pasquier, D. Marcotte, Application of deconvolution to interpretation of distributed thermal response test (DTRT) and to determination of thermal conductivity profiles, Appl. Therm. Eng. 236 (2024) 121680.
[32] A.R. Puttige, S. Andersson, R. Östin, T. Olofsson, Improvement of borehole heat exchanger model performance by calibration using measured data, J. Build. Perform. Simul. 13 (2020) 430–442.
[33] H. Soltan Mohammadi, L.M. Ringel, C. Bott, P. Bayer, Adaptive management of borehole heat exchanger fields under transient groundwater flow conditions, Renew. Energy 234 (2024) 121060, https://doi.org/10.1016/j.renene.2024.121060.
[34] I. Cupeiro Figueroa, M. Cimmino, J. Drgoňa, L. Helsen, Fluid temperature predictions of geothermal borefields using load estimations via state observers, J. Build. Perform. Simul. 14 (2021) 1–19.
[35] Y. Shoji, T. Katsura, K. Nagano, Improvement of accuracy with uncertainty quantification in the simulation of a ground heat exchanger by combining model prediction and observation, Geothermics 107 (2023) 102611, https://doi.org/10.1016/j.geothermics.2022.102611.
[36] W. Choi, H. Kikumoto, R. Choudhary, R. Ooka, Bayesian inference for thermal response test parameter estimation and uncertainty assessment, Appl. Energy 209 (2018) 306–321.
[37] W. Choi, H. Kikumoto, R. Ooka, Probabilistic uncertainty quantification of borehole thermal resistance in real-world scenarios, Energy 254 (2022) 124400.
[38] W. Choi, K. Menberg, H. Kikumoto, Y. Heo, R. Choudhary, R. Ooka, Bayesian inference of structural error in inverse models of thermal response tests, Appl. Energy 228 (2018) 1473–1485.
[39] K. Menberg, Y. Heo, R. Choudhary, Influence of error terms in Bayesian calibration of energy system models, J. Build. Perform. Simul. 12 (2019) 82–96.
[40] P. Pasquier, D. Marcotte, Robust identification of volumetric heat capacity and analysis of thermal response tests by Bayesian inference with correlated residuals, Appl. Energy 261 (2020) 114394.
[41] E. Shin, Y. Kim, Y.-S. Kim, S. Lee, W. Choi, Dynamic management of ground thermal response uncertainty through temporal analysis of parameter sensitivity, Appl. Energy 376 (2024) 124267.
[42] B. Zhang, K. Gu, P. Bayer, H. Qi, B. Shi, B. Wang, et al., Estimation of groundwater flow rate by an actively heated fiber optics based thermal response test in a grouted borehole, Water Resour. Res. 2023;59:e2022WR032672.
[43] H. Gebhardt, H. Soltan Mohammadi, A. Ebert, C. Bott, A. Visser, P. Bayer, High-resolution monitoring and simulation of the temperatures in a borehole heat exchanger field over multiple years, doi:10.22488/okstate.24.000019.
[44] S. Erol, B. François, Efficiency of various grouting materials for borehole heat exchangers, Appl. Therm. Eng. 70 (2014) 788–799, https://doi.org/10.1016/j.applthermaleng.2014.05.034.
[45] S. Erol, B. François, Multilayer analytical model for vertical ground heat exchanger with groundwater flow, Geothermics 71 (2018) 294–305, https://doi.org/10.1016/j.geothermics.2017.09.008.
[46] W.R. Gilks, S. Richardson, D. Spiegelhalter, Markov chain Monte Carlo in practice, CRC Press, 1995.
[47] S. Brooks, A. Gelman, G. Jones, X.-L. Meng, Handbook of Markov Chain Monte Carlo, CRC Press, 2011.
[48] J. Goodman, J. Weare, Ensemble samplers with affine invariance, Commun. Appl. Math. Comput. Sci. 5 (2010) 65–80.
[49] J. Hecht-Méndez, M. De Paly, M. Beck, P. Bayer, Optimization of energy extraction for vertical closed-loop geothermal systems considering groundwater flow, Energy Convers Manag 66 (2013) 1–10, https://doi.org/10.1016/j.enconman.2012.09.019.
[50] J.A. Christen, C. Fox, A general purpose sampling algorithm for continuous distributions (the t-walk) 2010.
[51] A. Grinsted, Affine Invariant Ensemble Markov Chain Monte Carlo Sampler. https://github.com/grinsted/gwmcmc.
[52] V. Roy, Convergence diagnostics for markov chain monte carlo, Annu Rev Stat Its Appl 7 (2020) 387–412.